Title

Matrix Rigidity Controls Epithelial-Mesenchymal Plasticity and Tumor Metastasis via a Mechanoresponsive EPHA2/LYN Complex

Journal

Developmental Cell, 54(3)

ISSN

1534-5807

Authors

Fattet, Laurent
Jung, Hae-Yun
Matsumoto, Mike W
et al.

Publication Date

2020-08-01

DOI

10.1016/j.devcel.2020.05.031

Peer reviewed

Article

Developmental Cell

Matrix Rigidity Controls Epithelial-Mesenchymal Plasticity and Tumor Metastasis via a Mechanoresponsive EPHA2/LYN Complex

Highlights

- High ECM stiffness activates LYN kinase to promote EMT and invasion
- LYN directly phosphorylates TWIST1 to promote nuclear localization of TWIST1
- High ECM stiffness promotes ligand-independent EPHA2 signaling to activate LYN
- EPHA2/LYN axis promotes breast tumor invasion and metastasis

Authors

Laurent Fattet, Hae-Yun Jung, Mike W. Matsumoto, ..., Adam J. Engler, Elena B. Pasquale, Jing Yang

Correspondence

jingyang@ucsd.edu

In Brief

Fattet et al. identified a EPHA2/LYN/TWIST1 signaling cascade activated by mechanical forces from the extracellular matrix to promote epithelial-mesenchymal transition and cell invasion. They demonstrate that activation of this mechanotransduction pathway promotes breast tumor invasion and metastasis and is involved in human breast cancer metastasis.

Fattet et al., 2020, Developmental Cell *54*, 1–15
August 10, 2020
https://doi.org/10.1016/j.devcel.2020.05.031

CellPress

Developmental Cell

CellPress

Article

Matrix Rigidity Controls Epithelial-Mesenchymal Plasticity and Tumor Metastasis via a Mechanoresponsive EPHA2/LYN Complex

Laurent Fattet,[1] Hae-Yun Jung,[1] Mike W. Matsumoto,[2] Brandon E. Aubol,[1] Aditya Kumar,[3] Joseph A. Adams,[1] Albert C. Chen,[3] Robert L. Sah,[3] Adam J. Engler,[3] Elena B. Pasquale,[2] and Jing Yang[1,4,5,*]

[1]Department of Pharmacology, University of California, San Diego, San Diego, 9500 Gilman Drive, La Jolla, CA 92093, USA
[2]Cancer Center, Sanford Burnham Prebys Medical Discovery Institute, San Diego, La Jolla, CA 92037, USA
[3]Department of Bioengineering, University of California, San Diego, San Diego, 9500 Gilman Drive, La Jolla, CA 92093, USA
[4]Moores Cancer Center, Department of Pediatrics, University of California, San Diego, San Diego, 3855 Health Sciences Drive, La Jolla, CA 92093, USA
[5]Lead Contact
*Correspondence: jingyang@ucsd.edu
https://doi.org/10.1016/j.devcel.2020.05.031

SUMMARY

Mechanical cues from the extracellular matrix (ECM) regulate various cellular processes via distinct mechanotransduction pathways. In breast cancer, increased ECM stiffness promotes epithelial-to-mesenchymal transition (EMT), cell invasion, and metastasis. Here, we identify a mechanosensitive EPHA2/LYN protein complex regulating EMT and metastasis in response to increasing ECM stiffness during tumor progression. High ECM stiffness leads to ligand-independent phosphorylation of ephrin receptor EPHA2, which recruits and activates the LYN kinase. LYN phosphorylates the EMT transcription factor TWIST1 to release TWIST1 from its cytoplasmic anchor G3BP2 to enter the nucleus, thus triggering EMT and invasion. Genetic and pharmacological inhibition of this pathway prevents breast tumor invasion and metastasis *in vivo*. In human breast cancer samples, activation of this pathway correlates with collagen fiber alignment, a marker of increasing ECM stiffness. Our findings reveal an EPHA2/LYN/TWIST1 mechanotransduction pathway that responds to mechanical signals from the tumor microenvironment to drive EMT, invasion, and metastasis.

INTRODUCTION

Mechanical forces from the extracellular matrix (ECM) have emerged as critical regulators of embryo morphogenesis, tissue remodeling, and tumor invasion and metastasis. During tumor development, increased deposition, modification and remodeling of the ECM generate a highly fibrotic tumor microenvironment with increased matrix rigidity, which is associated with poor patient prognosis (Wei et al., 2015; Chang et al., 2013; Mujtaba et al., 2013; Lu et al., 2012; Levental et al., 2009; Paszek et al., 2005; Boyd et al., 2002; Hasebe et al., 2002; Colpaert et al., 2001). Mechanical cues have been shown to impact diverse cellular processes including cell proliferation, survival and invasion (Martino et al., 2018; Paszek et al., 2005) by activating numerous mechanotransduction pathways, many of which are currently unknown.

Epithelial-to-mesenchymal transition (EMT) is a highly conserved developmental process aberrantly reactivated during tumor progression to provide epithelial tumor cells with the ability to invade and disseminate, while its reversion favors the outgrowth of metastatic lesions (Brabletz et al., 2018; Tsai et al., 2012). The plasticity of the EMT program suggests that EMT is dynamically regulated in response to extracellular signals from the microenvironment at the primary tumor site and distant organs. Using a widely used collagen-coated polyacrylamide hydrogel system in a three-dimensional (3D) Matrigel overlay culture system, we previously reported that high ECM stiffness promotes EMT and breast cancer metastasis via nuclear localization of the EMT transcription factor TWIST1, which can potently induce EMT and ECM degradation to promote efficient cell invasion and metastatic dissemination (Wei et al., 2015; Eckert et al., 2011; Yang et al., 2004). Expression of nuclear TWIST1 protein in tumor cells is significantly correlated with metastasis occurrence and decreased survival in breast cancer patients (Eckert et al., 2011). Mechanistically, high matrix stiffness releases TWIST1 from its cytoplasmic anchor protein G3BP2 to enter the nucleus and drive EMT-associated transcription (Wei et al., 2015). Consistent with this, a recent *in vivo* study shows that high tissue stiffness promotes EMT to trigger neural crest migration (Barriga et al., 2018). These studies together underscore a highly conserved role of matrix stiffness in driving EMT during both embryo morphogenesis and tumor metastasis.

Currently, the upstream mechanotransduction pathway transmitting mechanical cues from ECM to regulate TWIST1 and EMT is largely unknown. Here, we decipher the molecular links between increasing ECM stiffness and EMT and uncover a previously unknown pathway connecting an EPHA2/LYN mechanoresponsive protein complex with TWIST1 in regulating epithelial-mesenchymal plasticity and breast tumor metastasis.

Please cite this article in press as: Fattet et al., Matrix Rigidity Controls Epithelial-Mesenchymal Plasticity and Tumor Metastasis via a Mechanoresponsive EPHA2/LYN Complex, Developmental Cell (2020), https://doi.org/10.1016/j.devcel.2020.05.031

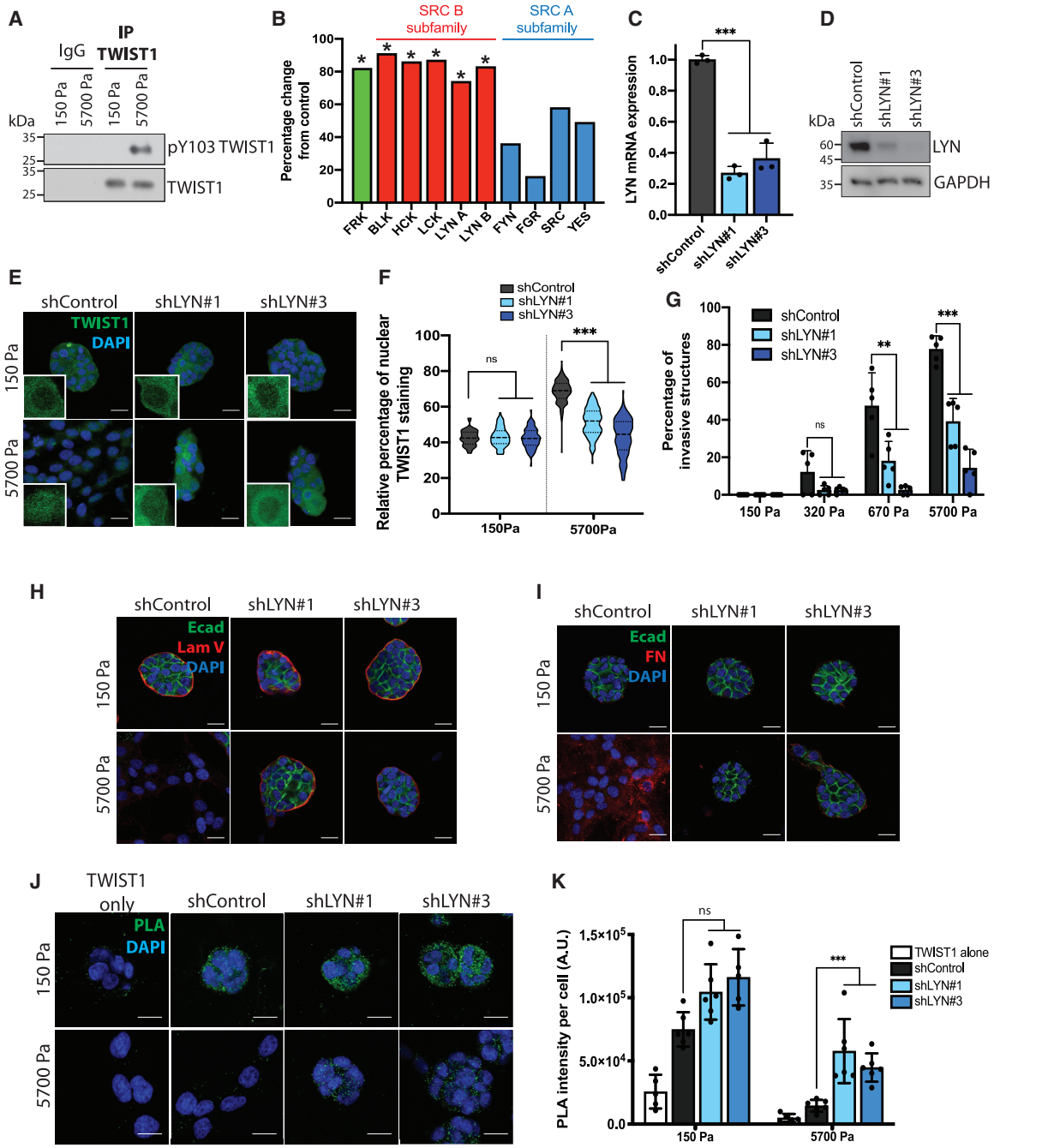

Figure 1. The LYN Kinase Is Essential for TWIST1 Nuclear Localization and EMT in Response to Increasing ECM Stiffness

(A) MCF10A cells were grown on 3D-PA gels with different rigidities for 5 days. Lysates were subjected to TWIST1 immunoprecipitation and immunoblotted as indicated.

(B) Radiometric kinase screening assay.* shows significance (CFC > 70%)

(C) qPCR analysis in MCF10A cells. Data are presented as mean ± SD, dots represent technical replicates.

(D) WB on lysates from MCF10A cells as indicated.

(E) Control or LYN-silenced MCF10A cells were grown on 3D-PA gels for 5 days, fixed, and immunostained for TWIST1 (green) and DAPI (blue). Inserts show higher magnification images.

(F) TWIST1 nuclear staining in (E) is presented as percent of total TWIST1 staining on a violin plot showing the distribution of the data with the median (hyphen line) and quartiles (dotted line).

(G) Control or LYN-silenced MCF10A cells were grown on 3D-PA gels for 5 days. Invasive structures were quantified and represented as percentages of total structures. Data are presented as mean ± SD, dots represent individual fields.

(legend continued on next page)

Please cite this article in press as: Fattet et al., Matrix Rigidity Controls Epithelial-Mesenchymal Plasticity and Tumor Metastasis via a Mechanoresponsive EPHA2/LYN Complex, Developmental Cell (2020), https://doi.org/10.1016/j.devcel.2020.05.031

RESULTS

The LYN Kinase Is Essential for High ECM Stiffness-Induced EMT and Invasion

To investigate mechanoresponsive regulation of EMT in breast cancer metastasis, we tested the hypothesis that phosphorylation of TWIST1 on tyrosine 103 (Y103) could release it from its cytoplasmic anchor G3BP2 to drive EMT. We immunoprecipitated endogenous TWIST1 from human MCF10A and mouse Eph4Ras mammary epithelial cells (MECs) cultured in the 3D hydrogel Matrigel system with calibrated elastic moduli ranging from the ~150 Pascals (Pa) of normal mammary glands to the ~5,700 Pa of breast tumor tissues (Johnson et al., 2007; Paszek et al., 2005). Using a phospho-Y103-specific antibody, we found that both endogenous human and mouse TWIST1 proteins are specifically phosphorylated on Y103 at 5,700 Pa, but not at 150 Pa (Figures 1A and S1A). Y103 phosphorylation is correlated with stiffness-induced TWIST1 dissociation from its cytoplasmic anchor G3BP2 (Figure S1B) and can disrupt the TWIST1/G3BP2 interaction (Wei et al., 2015). To identify the kinase responsible for TWIST1 phosphorylation on Y103 in response to high stiffness, we performed a screen of 73 tyrosine kinases for their ability to phosphorylate the Y103 motif (Figure S1C). Fourteen protein kinases were scored positive based on moderate (>10,000 cpm) to high (>40,000 cpm) levels of phosphorylation of a TWIST1 peptide containing Y103 and on high specificity (>70% higher phosphorylation of the Y103 peptide compared with a Y103F mutant peptide). Interestingly, all five Rous sarcoma oncogene (SRC) B subfamily kinases (FRK, BLK, HCK, LCK, and LYN), but none of the SRC A subfamily kinases (FYN, FGR, SRC, and YES), scored positive, suggesting a certain degree of specificity in TWIST1 phosphorylation on Y103 (Figure 1B).

We next determined the requirement of 14 candidates on TWIST1 nuclear localization and TWIST1/G3BP2 interaction. Among the candidate kinases whose expression is detectable in MECs (Figure S1D), only knockdown of LYN (Figures 1C, 1D, S1E, and S1F) inhibited TWIST1 nuclear translocation and tumor cell invasion in both mouse and human organoids grown in the 5,700 Pa hydrogels (Figures 1E, 1G, S1G, and S1J). Unlike control cells, MCF10A cells with LYN knockdown formed acini-like structures and did not undergo partial EMT nor invade at 5,700 Pa, as shown by E-cadherin and fibronectin staining, and retained basement membrane integrity as shown by laminin V staining (Figures 1H and 1I). We observed strong endogenous TWIST1/G3BP2 interaction in the cytoplasm of control cells at 150 Pa, which was lost at 5,700 Pa (Figures 1J, 1K, S1J, and S1K). In contrast, MCF10A cells with LYN knockdown maintained cytoplasmic proximity ligation assay (PLA) signals at 5,700 Pa. These results demonstrate an essential role of LYN in disrupting TWIST1 cytoplasmic sequestration by G3BP2, resulting in TWIST1 nuclear localization, EMT and invasion.

High ECM Stiffness Activates LYN to Directly Phosphorylate TWIST1 and Drive EMT and Invasion

We next ask whether the LYN kinase is activated to directly phosphorylate Y103 on TWIST1 at high stiffness, thus affecting the G3BP2-binding domain (Figure 2A). *In vitro* phosphorylation assays using TWIST1 wild type (WT) and Y103F mutant with recombinant active LYN showed significant increase of ^{32}P incorporation in TWIST1 WT compared with the Y103F mutant (Figures 2B and S2A). Both recombinant LYN and endogenous LYN immunoprecipitates from MCF10A cells effectively phosphorylate TWIST1 on Y103 (Figure 2C). Both LYN WT and the constitutively active Y508F mutant, but not the kinase-deficient Y397F mutant, can phosphorylate Y103 (Figure S2B). Furthermore, expression of LYN WT, but not the kinase-deficient Y397F mutant or other candidate kinases from the original screen, inhibited the interaction between TWIST1 and G3BP2 in MCF10A, MCF10DCIS, and Eph4Ras cells (Figures 2D and S2C–S2E). These results show that LYN can directly phosphorylate TWIST1 on Y103.

To determine the activation status of LYN in response to ECM stiffening, we immunoprecipitated endogenous human and mouse LYN from MCF10A, MCF10DCIS, and Eph4Ras organoids grown at various rigidities and found that Y397 phosphorylation in the LYN activation loop (corresponding to Y416 in SRC) was significantly higher at 5,700 Pa than at 150 Pa (Figures 2E–2H, S2F, and S2G). Importantly, endogenous LYN immunoprecipitated from MCF10A cells at 5,700 Pa, but not at 150 Pa, effectively phosphorylates TWIST1 on Y103, which indicates that high stiffness activates the LYN kinase to phosphorylate TWIST1 on Y103 (Figure 2I). Consistent with these data, the dual LYN and Bcr-Abl inhibitor bafetinib blocked phosphorylation of endogenous TWIST1 on Y103 at 5,700 Pa and inhibited the ability of immunoprecipitated endogenous LYN to phosphorylate TWIST1 on Y103 *in vitro* (Figures 2J–2L). The specificity of LYN in phosphorylating Y103 is further demonstrated by our finding that SRC is not activated and does not phosphorylate TWIST1 on Y103 at high stiffness (Figures 2M–2O). Together, these results strongly support the notion that LYN, but not other SRC family kinases, is specifically activated at high stiffness and directly phosphorylates TWIST1 on Y103 to release TWIST1 from its cytoplasmic anchor G3BP2, thus promoting EMT and invasion.

LYN Inhibition Prevents ECM Stiffness-Induced Cell Invasion and Metastatic Dissemination *In Vivo*

We next performed pharmacologic inhibition of LYN kinase to determine whether LYN could serve as a therapeutic target to inhibit ECM stiffness-induced tumor invasion and metastasis. Treating MCF10A 3D cultures with the LYN/Bcr-Abl dual inhibitor bafetinib, but not the Bcr-Abl-specific inhibitor nilotinib, decreased LYN phosphorylation on Y397 and inhibited ECM

(H and I) Control or LYN-silenced MCF10A cells were grown on 3D-PA gels for 5 days, fixed, and immunostained for E-cadherin (green), DAPI (blue) and (H) laminin V (LamV, red) or (I) fibronectin (FN, red).

(J) Control or LYN-silenced MCF10A cells were grown on 3D-PA gels for 5 days, fixed, and PLA (green dots) was performed to detect TWIST1-G3BP2 endogenous interaction, DAPI is in blue.

(K) Quantification of the PLA intensity per cell. a.u., arbitrary units. Data are presented as mean ± SD, dots represent individual fields.

***$p < 0.001$; **$p < 0.01$; ns, not significant. Scale bar represents 25 μm.

See also Figure S1.

Please cite this article in press as: Fattet et al., Matrix Rigidity Controls Epithelial-Mesenchymal Plasticity and Tumor Metastasis via a Mechanoresponsive EPHA2/LYN Complex, Developmental Cell (2020), https://doi.org/10.1016/j.devcel.2020.05.031

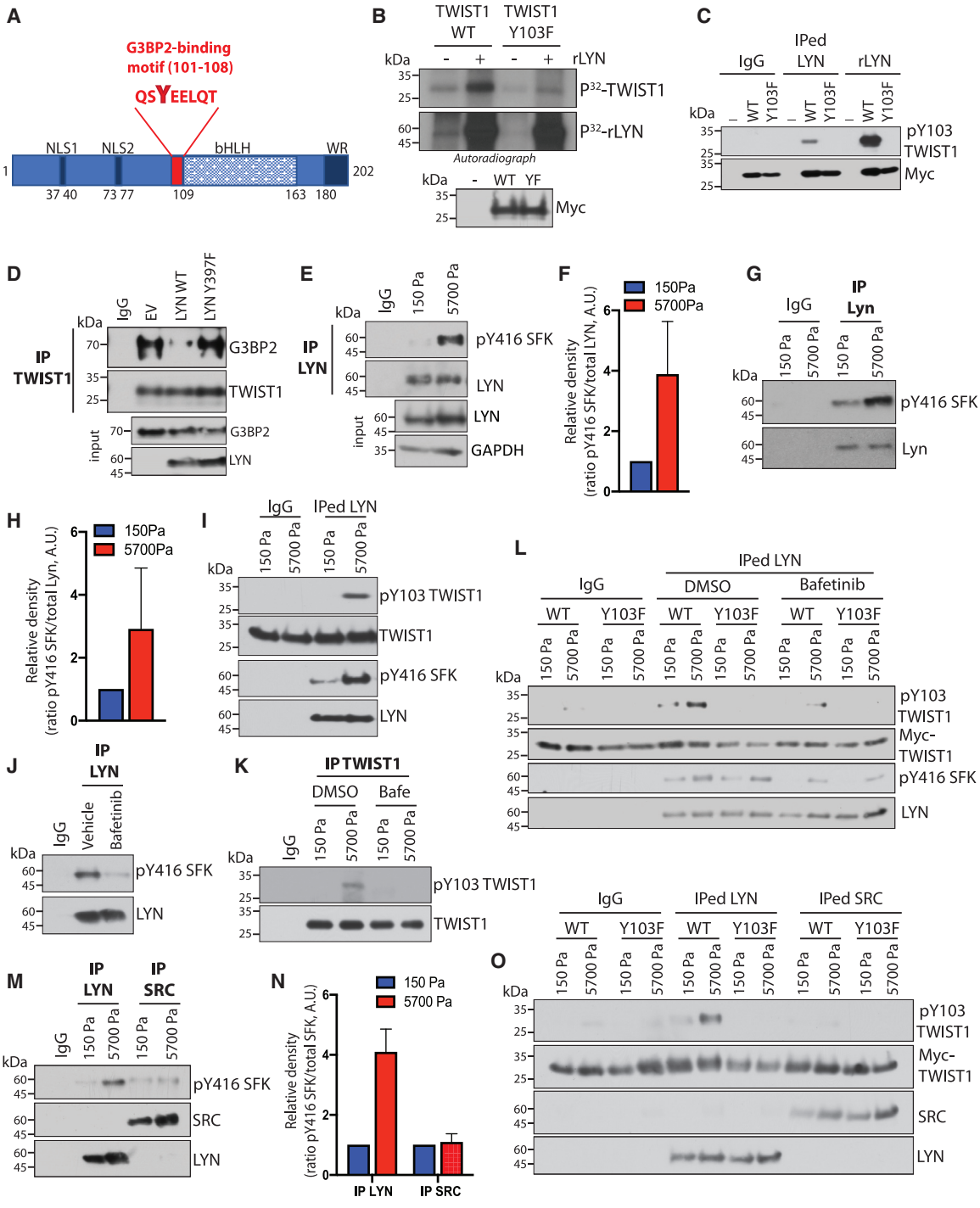

Figure 2. The LYN Kinase Is Activated and Directly Phosphorylates TWIST1 on Y103 to Drive Invasion in Response to Increasing ECM Stiffness

(A) Schematic representation of TWIST1 domain structure. The G3BP2-binding domain is highlighted in red. Amino acid numbers are indicated. NLS, nuclear localization signal; Bhlh, basic helix-loop-helix; WR, tryptophan arginine.

(B) Autoradiograph showing kinase assay.

(C) Cold *in vitro* kinase assay. Reactions were immunoblotted as indicated.

(D) MCF10A cells expressing WT or kinase-deficient (Y397F) LYN were subjected to TWIST1 immunoprecipitation and immunoblotted as indicated.

(E) Lysates from 3D-cultured MCF10A cells were subjected to LYN immunoprecipitation and immunoblotted as indicated.

(F) Protein amounts in (E) were quantified by densitometry (presented as the ratio of phospho-Y416 to total LYN levels).

(G) Lysates from 3D-cultured Eph4Ras cells were subjected to Lyn immunoprecipitation and immunoblotted as indicated.

(H) Relative protein levels in (G) were quantified by densitometry (presented as the ratio of phospho-Y416 to total Lyn levels).

(legend continued on next page)

Please cite this article in press as: Fattet et al., Matrix Rigidity Controls Epithelial-Mesenchymal Plasticity and Tumor Metastasis via a Mechanoresponsive EPHA2/LYN Complex, Developmental Cell (2020), https://doi.org/10.1016/j.devcel.2020.05.031

stiffness-induced cell invasion (Figures 2J, 3A, and S3A). Moreover, bafetinib, but not nilotinib treatment, rescued endogenous TWIST1-G3BP2 interaction at 5,700 Pa (Figures 3B and 3C). In addition, bafetinib treatment inhibited ECM stiffness-induced changes of EMT markers (Figure 3D). Even short treatment with bafetinib (24 h) prevents TWIST1 nuclear translocation in response to ECM stiffness without affecting G3BP2 cytoplasmic localization (Figures 3E and 3F). This further supports our model in which LYN-directed TWIST1 phosphorylation allows TWIST1 to enter the nucleus in response to high ECM stiffness.

To investigate the role of LYN in tumor progression *in vivo*, we used the MCF10DCIS human breast tumor orthotopic xenograft model, which recapitulates the progression from ductal carcinoma *in situ* (DCIS) to invasive ductal carcinoma (IDC) when implanted in mammary fat pads (Miller et al., 2000). Both rheology and atomic force microscopy analysis showed that MCF10DCIS tumors are significantly stiffer than normal mammary glands (Figures 7A and 7B). These tumors at 8 weeks (which have largely progressed to invasive IDC and resulted in lung metastases) showed higher collagen contents than tumors at 4 weeks (which are mostly non-invasive and non-metastatic DCIS), a feature that is correlated to a higher tissue stiffness (Mujtaba et al., 2013; Hasebe et al., 2002; Colpaert et al., 2001) (Figures S3B–S3G). We injected GFP-labeled MCF10DCIS cells into the mammary fat pad of SCID mice to allow primary tumor development for 3 weeks and then treated the mice with either vehicle control or bafetinib for 3 weeks (Figure 3G). Daily administration of bafetinib affected neither body weight nor primary tumor weight (Figures 3H, S3H, and S3I). However LYN inhibition significantly blocked the progression from DCIS to IDC, as shown by a significant decrease in local and regional invasion compared with vehicle or nilotinib-treated mice (Figures 3I, 3J, S3J, and S3K). More importantly, LYN inhibition drastically reduced the presence of GFP+ metastatic nodules in the lungs (Figures 3K and 3L). These results indicate that LYN kinase activity is critical for ECM stiffness-induced tumor cell invasion and metastatic dissemination.

ECM Stiffness-Induced LYN Kinase Activation Requires the ephrin Receptor EPHA2

We next aim to uncover the molecular mechanism driving LYN kinase activation in response to high ECM stiffness. We first investigated the known integrin-mediated mechanotransduction pathways in stiffness-driven TWIST1 translocation. While a β1-integrin blocking antibody can prevent stiffness sensing and block TWIST1 nuclear localization at high stiffness (Wei et al., 2015), its exact action is complex since the blocking antibody also blocks the binding of β1-integrin to its ECM ligands and affects cell attachment (Park et al., 2006). Surprisingly, inhibition of the integrin-activated focal adhesion kinase (FAK) or the downstream effector kinase SRC, could not block nuclear translocation of TWIST1 observed at 5,700 Pa (Figure S4A). In addition, FAK inhibition did not prevent the disruption of endogenous interaction between TWIST1 and G3BP2 observed in MCF10A (Figures S4B–S4E) and Eph4Ras (Figures S4F and S4G) cells at 5,700 Pa. Furthermore, MCF10A cells expressing either WT or V737N mutant of β1-integrin, which is reported to mimic stiffness-induced integrin clustering (Laklai et al., 2016), did not show any effect on TWIST1 translocation or TWIST1/G3BP2 interaction (Figures S4H–S4J). These results suggest that while integrins are required for ECM binding to transmit mechanical cues, additional signaling pathways are required to activate the LYN kinase in response to increased stiffness.

To identify mechano-regulators of LYN, we immunoprecipitated LYN from MCF10A 3D cultures on soft and stiff matrices and subjected the samples to liquid chromatography-tandem mass spectrometry (LC-MS/MS). Among all the hits, we focused on receptor kinases, given their likely roles in activating LYN in response to extracellular signals. The ephrin receptor, EPHA2, was the top candidate that selectively binds to LYN at 5,700 Pa compared with 150 Pa (Figures S5A and S5B). Co-immunoprecipitation experiments confirmed stiffness-dependent interaction between LYN and EPHA2 (Figures 4A and 4B). The specificity of this interaction is further supported by the fact that closely related EPHA family members EPHA1 and EPHA4 do not bind to LYN (Figures S5C and S5D). Like other SFKs, LYN activity is regulated by the phosphorylation status on both Y397 (activating site) and Y508 (inhibitory site), which tightly controls LYN conformation and accessibility to substrates (Thomas and Brugge, 1997). We performed sequential immunoprecipitation of endogenous EPHA2 and then LYN. The results show that the EPHA2-bound fraction of LYN lacks any detectable Y508 phosphorylation, while phosphorylation on the Y397 activation site was readily detected at 5,700 Pa (Figure 4C), strongly suggesting that the EPHA2-bound LYN is in an open conformation and enzymatically active at high matrix stiffness. Indeed, we found that the LYN Y397F kinase-deficient mutant binds less to EPHA2 than LYN WT (Figure S5E). In contrast, the LYN Y508F mutant, which is in an open conformation and constitutively active (Cartwright et al., 1987; Kmiecik and Shalloway, 1987), binds to EPHA2 better than LYN WT.

To test the functional significance of EPHA2 in TWIST1 mechanoresponsive signaling, we knocked down EPHA2 in both MCF10A and Eph4Ras cells (Figures 4D and S5F). Loss of

(I) LYN immunoprecipitates from 3D-cultured MCF10A cells were used for cold *in vitro* kinase assay, with WT or Y103F mutant TWIST1 pulled down from 293T cells. Reactions were immunoblotted as indicated.

(J) MCF10A cells were treated with 1 μM bafetinib or vehicle control (DMSO). Lysates were subjected to LYN immunoprecipitation and immunoblotted as indicated.

(K) MCF10A cells were grown on 3D-PA gels for 5 days, treated with 1 μM bafetinib (Bafe) or vehicle control (DMSO). Lysates were subjected to TWIST1 immunoprecipitation and immunoblotted as indicated.

(L) LYN immunoprecipitates from 3D-cultured MCF10A cells were used for cold *in vitro* kinase assays, in presence of 1 μM bafetinib or vehicle control (DMSO). Reactions were immunoblotted as indicated.

(M) Lysates from 3D-cultured MCF10A cells were subjected to LYN or SRC immunoprecipitation and immunoblotted as indicated.

(N) Relative protein levels in (M) were quantified by densitometry (presented as the ratio of phospho-Y416 to total LYN/SRC levels).

(O) LYN or SRC immunoprecipitates from 3D-cultured MCF10A cells were used for cold *in vitro* kinase assay. Reactions were immunoblotted as indicated.

See also Figure S2.

Please cite this article in press as: Fattet et al., Matrix Rigidity Controls Epithelial-Mesenchymal Plasticity and Tumor Metastasis via a Mechanoresponsive EPHA2/LYN Complex, Developmental Cell (2020), https://doi.org/10.1016/j.devcel.2020.05.031

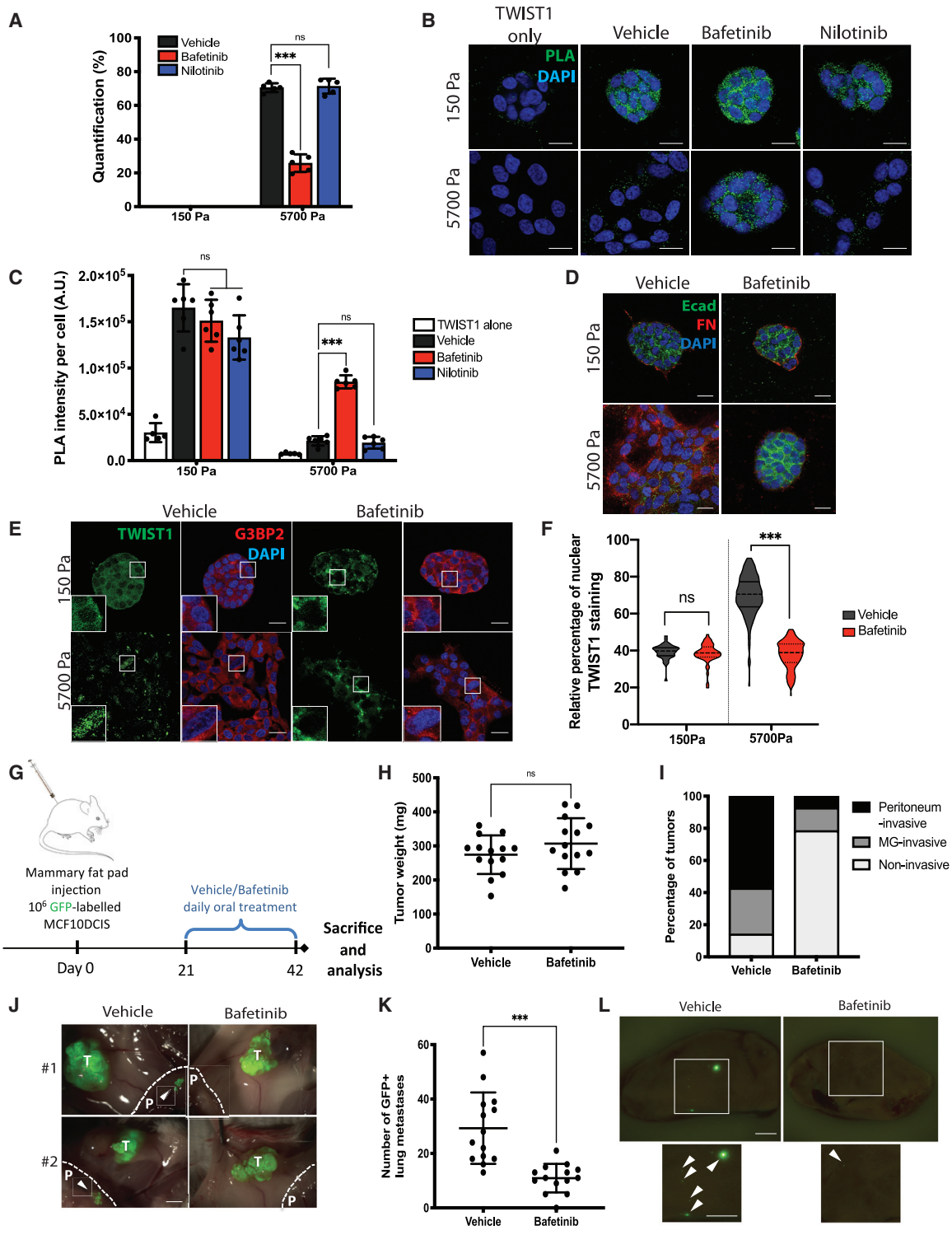

Figure 3. LYN Inhibition Prevents ECM Stiffness-Induced Cell Invasion and Metastatic Dissemination *In Vivo*

(A–F) MCF10A cells were grown on 3D-PA gels for 5 days in the presence of 1 μM bafetinib, nilotinib, or vehicle control.

(A) Invasive structures were quantified and represented as percentages of total structures. Data are presented as mean ± SD, dots represent individual fields.

(B) PLA (green dots) was performed to detect TWIST1-G3BP2 endogenous interaction, DAPI is in blue. Scale bar represents 25 μm.

(C) Quantification of the PLA intensity per cell in (B). a.u., arbitrary units. Data are presented as mean ± SD, dots represent individual fields.

(D) Cells were immunostained for E-cadherin (green), DAPI (blue), and FN (red). Scale bar represents 25 μm.

(E) Cells were immunostained for TWIST1 (green), G3BP2 (red), and DAPI (blue). Scale bar represents 25 μm. Inserts show high-magnification images.

(legend continued on next page)

Please cite this article in press as: Fattet et al., Matrix Rigidity Controls Epithelial-Mesenchymal Plasticity and Tumor Metastasis via a Mechanoresponsive EPHA2/LYN Complex, Developmental Cell (2020), https://doi.org/10.1016/j.devcel.2020.05.031

EPHA2 significantly reduced nuclear translocation of TWIST1, EMT induction, and cell invasion (Figures 4E–4H and S5G–S5J). We next investigated the importance of EPHA2 in metastatic dissemination in the MCF10DCIS xenograft model. Control tumors progress to IDC and present local invasion and lung metastases at 8 weeks post-implantation (Figures 4I–4L). Knockdown of EPHA2 drastically inhibited tumor invasion into the peritoneum and more importantly dissemination to the lungs, but only reducing primary tumor weight slightly (Figures 4I–4L and S5K). These results together identify EPHA2 as a key player in the mechanotransduction pathway that leads to LYN activation and TWIST1 nuclear translocation, thus triggering tumor invasion and metastasis in response to ECM stiffening.

High ECM Stiffness Activates Ligand-Independent EPHA2 Signaling to Promote EMT and Invasion

We next sought to understand how ECM stiffness regulates EPHA2 to activate LYN. EPHA2 can exert pro- or anti-tumorigenic activities depending on ligand binding (Pasquale, 2010). Ligand binding to EPHA2 is originally shown to reverse the malignant phenotype observed in EPHA2-overexpressing MECs (Zelinski et al., 2001). In the absence of ligands, EPHA2 can be phosphorylated on serine 897 (S897), triggering a non-canonical signaling that promotes tumor cell migration and metastasis through an unknown mechanism (Li et al., 2019; Zhou and Sakurai, 2017; Paraiso et al., 2015; Zhou et al., 2015; Miao et al., 2009). Ligand binding activates EPHA2 tyrosine kinase activity, suppresses S897 phosphorylation and blocks tumorigenesis by inhibiting extracellular signal-regulated kinase (ERK) signaling (Pasquale, 2010, 2008). Interestingly, we found that treatment with the ephrinA1-Fc ligand inhibited TWIST1 nuclear translocation and invasion at high stiffness (Figures 5A–5C and S6A). In 3D cultures, phosphorylation on S897, but not Y588, drastically increased at 5,700 Pa (Figure 5D). This drastic activation of EPHA2 non-canonical signaling in response to ECM stiffness could not be explained by mild decrease of the endogenous ephrinA1 ligand level (Figures S6B and S6C). Activation of EPHA2 canonical signaling using ephrinA1-Fc reduced EPHA2 S897 phosphorylation and prevented the interaction between LYN and EPHA2 as well as LYN activation (Figure 5E), further supporting the notion that matrix stiffness activates ligand-independent EPHA2 signaling via S897 phosphorylation.

We next analyzed the impact of EPHA2 S897 phosphorylation on LYN binding and found that the S897A mutation in EPHA2 inhibits the interaction between EPHA2 and LYN, whereas both EPHA2 WT and the K646M kinase-dead mutant interact with LYN (Figure 5F). We then knocked down EPHA2 in MCF10A cells to determine the ability of reconstituted EPHA2 WT and S897A (SA) mutant to rescue stiffness-induced cell invasion (Figure S6D). While EPHA2 WT and the K646M (KM) mutant were both able to restore ECM stiffness-induced LYN activation, TWIST1 nuclear translocation, and cell invasion, the S897A mutant completely failed to do so (Figures 5G–5K). These data strongly indicate that EPHA2 phosphorylation on S897 is required for stiffness-activated LYN/TWIST1 mechanotransduction.

EPHA2 was reported to be directly phosphorylated on S897 by the ERK/ribosomal S6 kinase (RSK) or AKT signaling in 2D culture (Li et al., 2019; Zhou et al., 2015; Miao et al., 2009). We found that EPHA2 non-canonical signaling triggered by ECM stiffness correlates with activation of the ERK and RSK kinases, but not AKT (Figures 6A and S6E). Consistent with these data, pharmacologic inhibition of ERK1/2, but not of AKT, inhibits RSK phosphorylation, ECM stiffness-dependent cell invasion and TWIST1 nuclear translocation (Figures 6B–6D). In addition, inhibition of RSK family members inhibited EPHA2 S897 phosphorylation and stiffness-induced cell invasion (Figures S6F and S6G). Supporting the role of LYN and RSK in regulating TWIST1 to impact EMT and invasion, knockdown of G3BP2 to allow TWIST1 nuclear translocation could significantly reverse the effect of LYN or RSK inhibition at high matrix stiffness (Figure S6G). We next knocked down the most abundant RSK family members and found that loss of RSK1, but not RSK2 or RSK3, drastically inhibited EPHA2 S897 phosphorylation, prevented ECM stiffness-induced LYN activation and recruitment to EPHA2, and inhibited cell EMT and invasion induced by increasing rigidities (Figures 6F–6I and S6H–S6L). Importantly, expression of a dominant-negative kinase-dead mutant of RSK1 (K94/447R) decreased EPHA2 S897 phosphorylation and prevented ECM stiffness-induced invasion and EMT (Figures S6M–S6P). In mice, we found that RSK1 knockdown strongly inhibited primary tumor invasion and lung metastasis, despite an increase of primary tumor growth (Figures 6J–6L). These comprehensive analyses indicate that high matrix stiffness activates ERK/RSK1-mediated EPHA2 non-canonical signaling to induce LYN activation, TWIST1 nuclear localization, and cell invasion (Figure 6M).

Activation of EPHA2 Non-canonical Signaling Correlates with Breast Tumor Progression and Metastasis

To understand whether ECM stiffness regulates EPHA2 and LYN in human breast cancers, shear rheology and force mapping by nanoscale atomic force microscopy (AFM) found a >10-fold increase in Young's modulus in MCF10DCIS tumors compared with normal mammary gland (Figures 7A and 7B). Importantly, DCIS samples showed a higher Y397 phosphorylation level in LYN immunoprecipitates (Figures 7C and 7D) and enhanced phosphorylation of EPHA2 on S897, suggesting the activation of LYN

(F) TWIST1 nuclear signal in (E) is presented as the percentage of total TWIST1 staining on a violin plot showing the distribution of the data with the median (hyphen line) and quartiles (dotted line).
(G) Schematic depicting the protocol used for *in vivo* experiments.
(H) Tumor weight (mg) at the end of the experiment are presented as mean ± SD, dots represent individual animals. n = 14 tumors per group.
(I) Local (mammary gland, MG) or regional (peritoneum) invasion of the primary tumor. Data are presented as percentage. N = 14 mice per group.
(J) Representative images of the primary tumor invasion (T, tumor; P, peritoneum). Arrow shows GFP-positive invasive tumor cells. Scale bar represents 5 mm.
(K) Lung metastatic burden presented as the number of GFP+ nodules in the lungs. Data are presented as mean ± SD, dots represent individual animals. N = 14 mice per group.
(L) Representative images. Arrows show metastatic tumor cells. Scale bar represents 1 mm.
***$p < 0.001$; ns, not significant.
See also Figure S3.

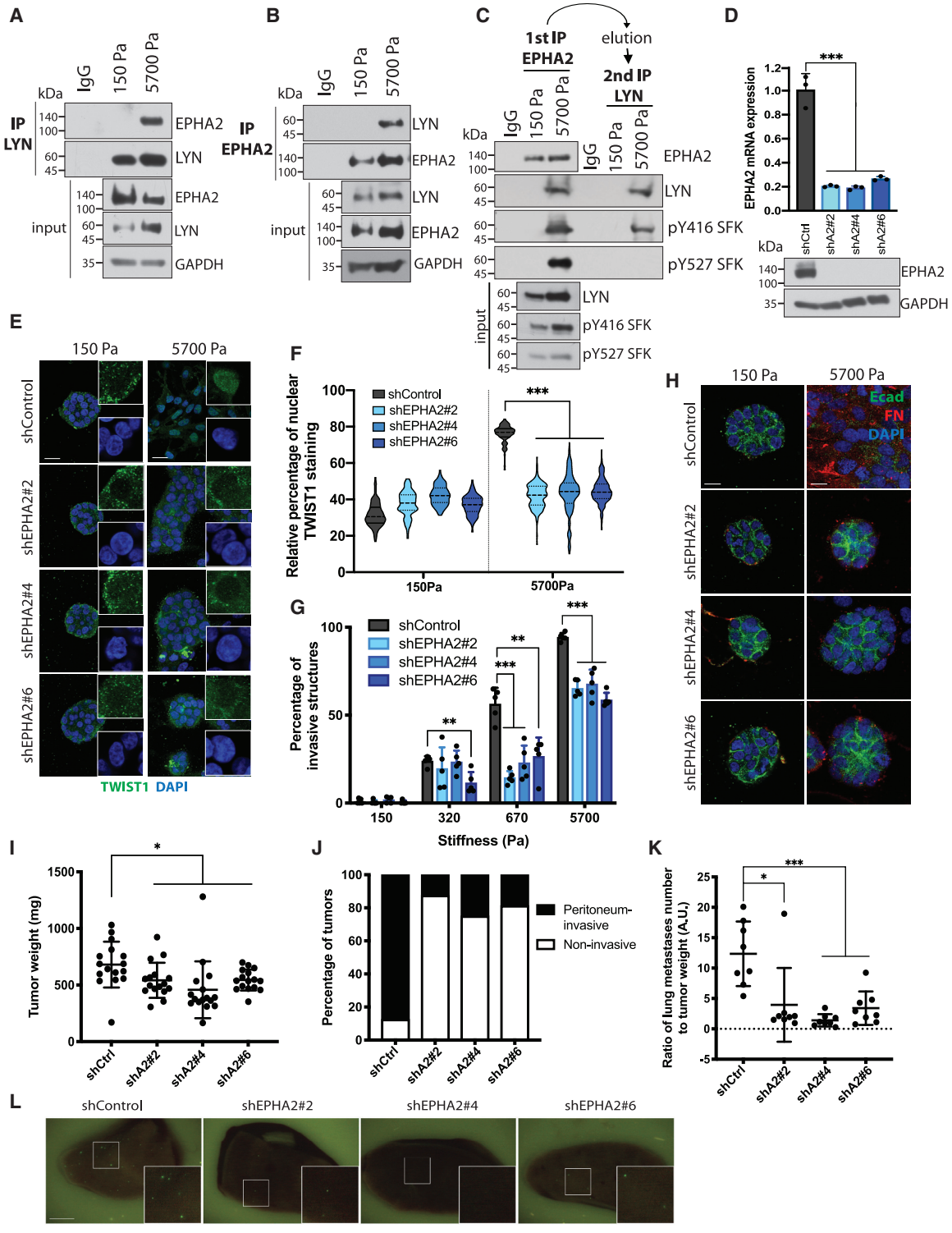

Figure 4. ECM Stiffness-Induced LYN Kinase Activation Requires the Ephrin Receptor EPHA2

(A and B) Lysates from 3D-cultured MCF10A cells were subjected to LYN (A) or EPHA2 (B) immunoprecipitation and immunoblotted as indicated.

(C) Lysates from 3D-cultured MCF10A cells were subjected to sequential immunoprecipitation and immunoblotted as indicated.

(D) Upper panel, qPCR analysis in MCF10A cells. Data are presented as mean ± SD, dots represent technical replicates. Lower panel, WB with lysate from MCF10A cells as indicated.

(E) Control or EPHA2-silenced MCF10A cells were grown on 3D-PA gels for 5 days and immunostained for TWIST1 (green) and DAPI (blue). Scale bar represents 25 μm. Inserts show high magnification.

(legend continued on next page)

Please cite this article in press as: Fattet et al., Matrix Rigidity Controls Epithelial-Mesenchymal Plasticity and Tumor Metastasis via a Mechanoresponsive EPHA2/LYN Complex, Developmental Cell (2020), https://doi.org/10.1016/j.devcel.2020.05.031

kinase and the non-canonical EPHA2 signaling pathway in tumor samples (Figures 7E and 7F). We next evaluated EPHA2 S897 phosphorylation by immunohistochemistry (Figure 7G) and collagen organization as a surrogate marker for tumor tissue stiffness by second-harmonic generation (SHG) imaging in a human breast tumor microarray (TMA) containing 197 stage III samples. SHG imaging analysis defined more compliant tumor samples with disorganized collagen, comparable with the normal breast tissue stiffness, intermediate tumors harboring mixed collagen structures, and stiffer tumors with straight and organized collagen fibers (Figure 7H). Consistent with previous studies, collagen organization in tumor samples correlated with recurrence-free survival as well as overall survival (Figures S7A and S7B). Interestingly, EPHA2 phosphorylation on S897 is significantly higher in tumors with more organized collagen structures, indicating stiffer breast tumors (Figures 7I and 7J). In addition, we analyzed the SHG data using previously described tumor-associated collagen signature (TACS1-3), which correlates with breast tumor aggressiveness (Provenzano et al., 2006). Such collagen signature analysis (Figure S7C) indicated an enrichment of EPHA2 phosphorylation on S897 in the TACS-3-containing aggressive breast tumors (Figures 7K and 7L). These results together show that non-canonical activation of EPHA2 correlates with tissue stiffening in human breast cancer.

DISCUSSION

Recent progress in mechanobiology has led to the identification of new mechanosensors and transmitters that convert mechanical signals from the extracellular compartment to biochemical pathways inside the cell (Broders-Bondon et al., 2018). We demonstrate here that kinases previously known to regulate axon guidance, cell motility, invasiveness and proliferation are utilized by the mechanotransduction machinery to promote TWIST1-mediated EMT and tumor metastasis in response to increasing matrix stiffness in breast tumors. The finding that LYN kinase specifically regulates this mechanoresponsive pathway led us to successfully inhibit tumor cell invasion *in vitro* and dissemination and metastasis *in vivo* in a model of DCIS to IDC tumor progression using the Bcr-Abl/LYN dual inhibitor bafetinib (INNO-406), previously shown to be safe and well tolerated in patients with chronic myelogenous leukemia in a phase 1 trial.

Focal adhesions are one of the first characterized molecular platforms that transmit mechanical cues from the ECM to the actin cytoskeleton via integrins and their associated kinases FAK and SRC. More recently, studies have identified additional RTKs, such as AXL and ROR2, in mechanotransduction (Yang et al., 2016). Our previous study showed that treatment with a β1-integrin-blocking antibody could block TWIST1 nuclear translocation and cell invasion in response to high stiffness. However, further mechanistic experiments using the V737N β1-integrin mutant, which mimics mechanoactivation of integrins (Laklai et al., 2016; Miroshnikova et al., 2016; Paszek et al., 2005), did not affect TWIST1 localization (Figures S4I–S4K). Inhibition of FAK or SRC did not affect ECM stiffness-dependent regulation of TWIST1 nuclear translocation (Figures S4A–S4H). We think that the different results obtained with the β1-integrin-blocking antibody versus FAK/SRC inhibitors is likely due to the fact that treatment with the β1-integrin blocking antibody reduces overall cell-ECM adhesion, thus generally preventing downstream mechanotransduction pathways. Our previous study (Wei et al., 2015) also revealed that mechanoregulation of TWIST1 is distinct from that of YAP/TAZ, which are responsive to changes in cell shape and actin cytoskeleton to promote cell proliferation (Dupont et al., 2011; Zhao et al., 2007). Instead, we identified EPHA2 and LYN as upstream mechanoregulators of TWIST1 and EMT. While we show that ERK and RSK1 are both required for activation of the EPHA2/LYN cascade, oncogenic Ras in both Eph4Ras and MCF10DCIS cells is not sufficient to promote invasion under low rigidities. These results suggest that a number of distinct sensors and transducers, many of which are currently unknown, might cooperate with the conventional integrin mechanotransduction to convert the matrix mechanical cue into TWIST1 phosphorylation and nuclear translocation to promote EMT and invasion. A number of integrins and stretch-activated ion channels are involved in mechanotransduction in various biological context (Majeski and Yang, 2016), future studies are needed to decipher their roles in the LYN/EPHA2/TWIST1 pathway.

Originally characterized as an axon guidance regulator, the EPH-ephrin system mediates cell-cell communication-dependent processes that are critical for embryonic morphogenesis, including germ layer separation (Rohani et al., 2011), neural crest cell migration (Smith et al., 1997) or vascular organization (Brantley-Sieders and Chen, 2004). The role of EPHA2 in mechanotransduction upstream of LYN and TWIST1 appears to be specific, since we did not find evidence implicating other EPH receptors expressed in MECs, including EPHA1, EPHA4, and EPHB1. In contrast to the classical response of EPHA2 to its ligands, we demonstrate here that ECM stiffening triggers EPHA2 S897 phosphorylation in a ligand-independent fashion. Interestingly, we show that ligand binding to EPHA2 inhibits stiffness-induced S897 phosphorylation, EMT and invasion. Given

(F) TWIST1 nuclear signal in (E) is presented as the percentage of total TWIST1 staining on a violin plot showing the distribution of the data with the median (hyphen line) and quartiles (dotted line).

(G) Quantification of the experiment in Figure S5G, expressed as percentage of invasive structures. Data are presented as mean ± SD, dots represent individual fields.

(H) Control or EPHA2-silenced MCF10A cells were grown on 3D-PA gels for 5 days and immunostained for E-cadherin (green), DAPI (blue), and FN (red). Scale bar represents 25 μm.

(I–L) GFP-labeled control or EPHA2-silenced MCF10DCIS cells were injected into the mammary gland of NOD/SCID mice. (I) Tumor weight (mg) at the experiment's endpoint. Data are presented as mean ± SD, dots represent individual tumors. n = 16 tumors per group. (J) Regional (peritoneum) invasion of the primary tumor is presented as the percentage of total primary tumors. N = 8 mice per group. (K) Lung metastatic burden is presented as the ratio of the number of GFP+ nodules in the lungs to tumor weight. a.u., arbitrary units. Data are presented as mean ± SD, dots represent individual animals. N = 8 mice per group. (L) Representative images. Scale bar represents 1 mm.

***$p < 0.001$; **$p < 0.01$; *$p < 0.05$.

See also Figures S4 and S5.

Please cite this article in press as: Fattet et al., Matrix Rigidity Controls Epithelial-Mesenchymal Plasticity and Tumor Metastasis via a Mechanoresponsive EPHA2/LYN Complex, Developmental Cell (2020), https://doi.org/10.1016/j.devcel.2020.05.031

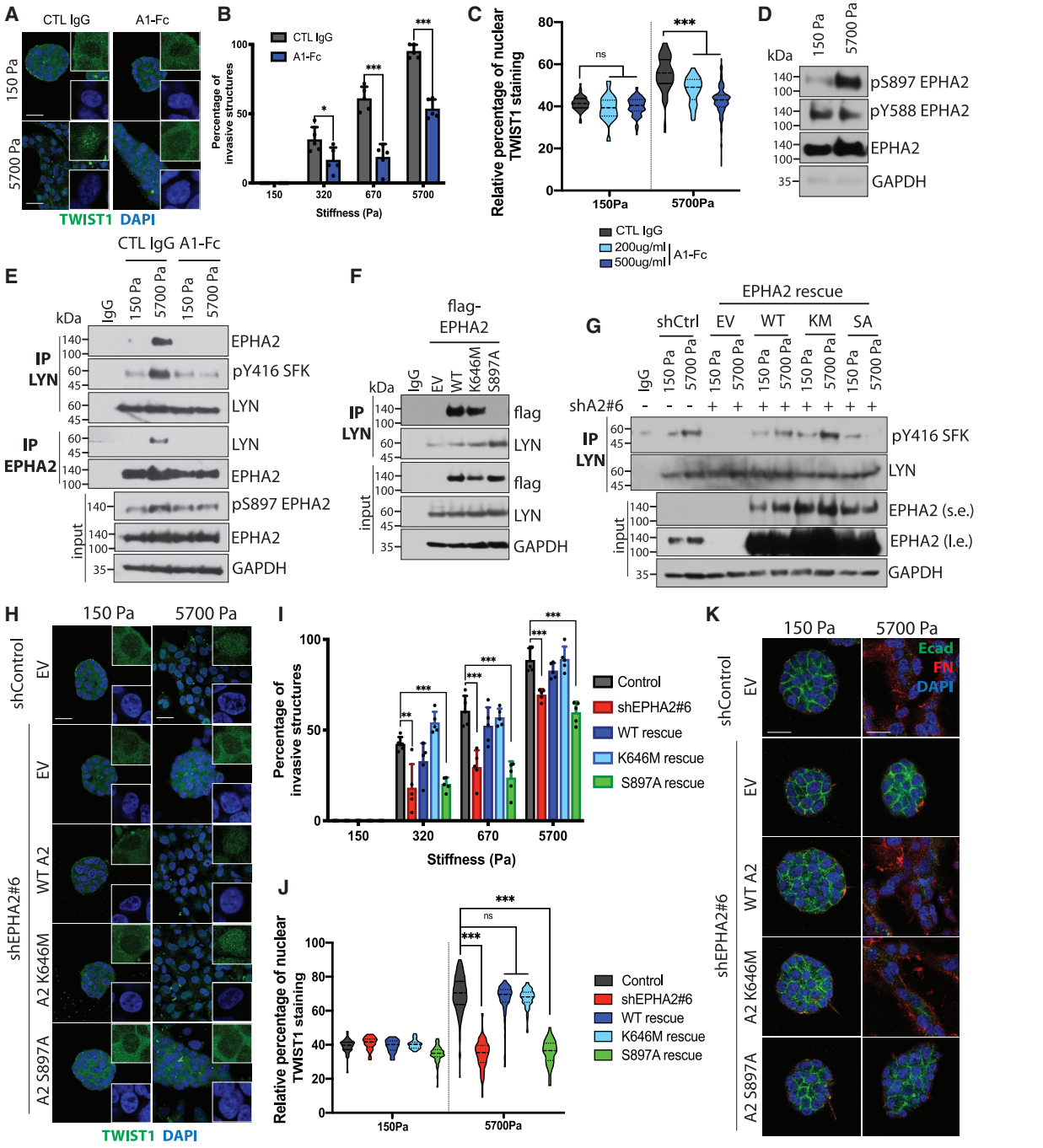

Figure 5. Ligand-Independent EPHA2 Signaling Promotes LYN Activation and Cell Invasion in Response to Increasing ECM Stiffness

(A–C) MCF10A cells were grown on 3D-PA gels for 5 days in presence of 400 μg/mL recombinant ephrinA1-Fc chimera or IgG control. (A) Cells were stained for TWIST1 (green) and DAPI (blue). Scale bar represents 25 μm. Inserts show high magnification. (B) Organoid phenotypes were quantified as percentage of invasive structures. Data are presented as mean ± SD, dots represent individual fields. (C) TWIST1 nuclear signal in (A) is presented as percentage of total TWIST1 staining on a violin plot showing the distribution of the data with the median (hyphen line) and quartiles (dotted line).

(D) Lysates from 3D-cultured MCF10A cells were immunoblotted as indicated.

(E) Lysates from 3D-cultured MCF10A cells, treated with 400 μg/mL recombinant ephrinA1-Fc chimera or IgG control, were subjected to LYN or EPHA2 immunoprecipitation and immunoblotted as indicated.

(F) Lysates from 293T cells were subjected to LYN immunoprecipitation and immunoblotted as indicated.

(G) Control or EPHA2-silenced MCF10A cells rescued for WT, kinase-dead (KM), or S897 phosphorylation defective mutant (SA) were grown on 3D-PA gels for 5 days. Lysates were subjected to LYN immunoprecipitation and immunoblotted as indicated.

(H) Control or EPHA2-silenced MCF10A cells rescued for WT, K646M, or S897A mutants of EPHA2 grown on 3D-PA gels for 5 days were stained for TWIST1 (green) and DAPI (blue). Scale bar represents 25 μm. Inserts show high-magnification images.

(legend continued on next page)

the important role of EPH receptors in diverse cell migration processes and axon guidance, we speculate that in the absence of biochemical cues, the signaling status of EPHA2 could be dictated by the mechanical properties of the ECM. Encountering ligands at the target site could switch off the mechanical-competent state of EPHA2 to stop cell migration. Therefore, during diverse cellular processes, extracellular biochemical and mechanical cues could switch on and off the same receptor to dictate distinct intracellular signaling responses and cellular behaviors, thus inserting a new mode of receptor regulation.

While SFKs share high similarities in their protein structures and substrate recognition, our results show that LYN, but not SRC, is uniquely activated in response to matrix stiffness and directly phosphorylates TWIST1 on Y103. LYN is ubiquitously expressed in many human tissues, including the mammary gland. However, to date, most studies on LYN have focused on its role in the hematopoietic system. The role of LYN in breast tumorigenesis is poorly understood and some recent research, in agreement with our data, suggests that LYN expression and/or splicing is important for breast cancer EMT and metastasis (Tornillo et al., 2018; Tabariès et al., 2015; Choi et al., 2010). A recent study reports that LYN regulates EMT and metastasis via the activation of the Vav-Rac1-PAK1 axis leading to SLUG stability (Thaper et al., 2017). Our current study provides both mechanistic and functional insights on how LYN kinase activity is activated by ECM stiffness to promote EMT and metastasis. The detailed molecular mechanism linking EPHA2 to LYN activation is currently under investigation. Comparing the structures and localization of LYN and SRC might provide clues on how high stiffness selectively activates LYN to promote TWIST1 phosphorylation and cell invasion. Targeting LYN using bafetinib in patients with collagen-dense breast tumors should be further evaluated as a promising approach to prevent tumor cell dissemination and metastasis using additional *in vivo* models as well as patient-derived xenografts.

Induction of EMT by matrix stiffness was first observed in human and mouse MECs to promote tumor invasion and then was shown to be also essential for neural crest migration in *Xenopus* (Barriga et al., 2018). Given the conserved roles of EMT and TWIST1 in embryo morphogenesis and tumor metastasis, we speculate that the EPHA2/LYN/TWIST1 mechanotransduction pathway described here is likely to operate not only in tumors but also during developmental EMT events.

STAR★METHODS

Detailed methods are provided in the online version of this paper and include the following:

- KEY RESOURCES TABLE
- RESOURCE AVAILABILITY
  - Lead Contact
  - Materials Availability
  - Data and Code Availability
- EXPERIMENTAL MODEL AND SUBJECT DETAILS
  - Cell Lines
  - Mouse Strain
- METHOD DETAILS
  - Cell Culture
  - DNA Constructs
  - Generation of Stable Cell Lines
  - Polyacrylamide Hydrogel Preparation
  - 3-dimensional (3D) Cell Culture
  - 3D Confocal Microscopy
  - Second Harmonic Generation Microscopy
  - Tumor Tissue Microarrays
  - Immunoprecipitation
  - Mass Spectrometry
  - Proximity Ligation Assay
  - Real-time PCR
  - *In Vitro* Phosphorylation Assay with Radioactive ATP
  - *In Vitro* Cold Phosphorylation Assay
  - Ni-NTA Purification
  - Tyrosine Kinases Screen
  - Strep-Tactin Pulldown
  - Rheology Measurement of Tumor Tissue Stiffness
  - Masson Trichrome Staining
  - Xenograft Tumor Assay
- QUANTIFICATION AND STATISTICAL ANALYSIS
  - Invasive Acini Quantification
  - TWIST1 Nuclear Staining Quantification
  - Quantification of IHC Signals from TMAs
  - Quantification of SHG Signals from TMAs
  - Statistical Analysis

SUPPLEMENTAL INFORMATION

Supplemental Information can be found online at https://doi.org/10.1016/j.devcel.2020.05.031.

ACKNOWLEDGMENTS

We thank members of the Yang lab, especially H. Majeski and D. Kim, for technical advice and helpful discussions. We thank the La Jolla Institute microscopy core, in particular Z. Mikulski for SHG imaging, M. Ghassemian at the UCSD mass spectrometry core as well as M. Makale for technical support and advice. We thank D. Shlaepfer for the FAK inhibitor, A. Burgoyne for AKT and ERK inhibitors, V. Weaver for the V737N integrin constructs, Y. Zhou for the pS897 EPHA2 IHC protocol, S. Taylor for RSK1 constructs, C. Dargemont for pEGFP-C1-G3BP2 construct, and M. Aumailley for anti-laminin V antibody. We thank the UCSD Shared Microscope Facility and UCSD Cancer Center Support grant P30 CA23100 from NCI. This work was supported by grants from NCI (1RO1CA168689, 1R01CA174869, 1R01CA206880, and 1R01CA236386) and from California Breast Cancer Research Program (24IB-0066) to J.Y., a pilot grant from Cancer Center Support grant P30

(I) Quantification of the data presented in Figure S5L is presented as percentage of invasive structures. Data are presented as mean ± SD, dots represent individual fields.
(J) TWIST1 nuclear signal in (H) is presented as the percentage of total TWIST1 staining on a violin plot showing the distribution of the data with the median (hyphen line) and quartiles (dotted line).
(K) Cells were immunostained for E-cadherin (green), DAPI (blue), and FN (red). Scale bar represents 25 μm.
***p < 0.001; **p < 0.01; *p < 0.05. ns, not significant.
See also Figures S5 and S6.

Please cite this article in press as: Fattet et al., Matrix Rigidity Controls Epithelial-Mesenchymal Plasticity and Tumor Metastasis via a Mechanoresponsive EPHA2/LYN Complex, Developmental Cell (2020), https://doi.org/10.1016/j.devcel.2020.05.031

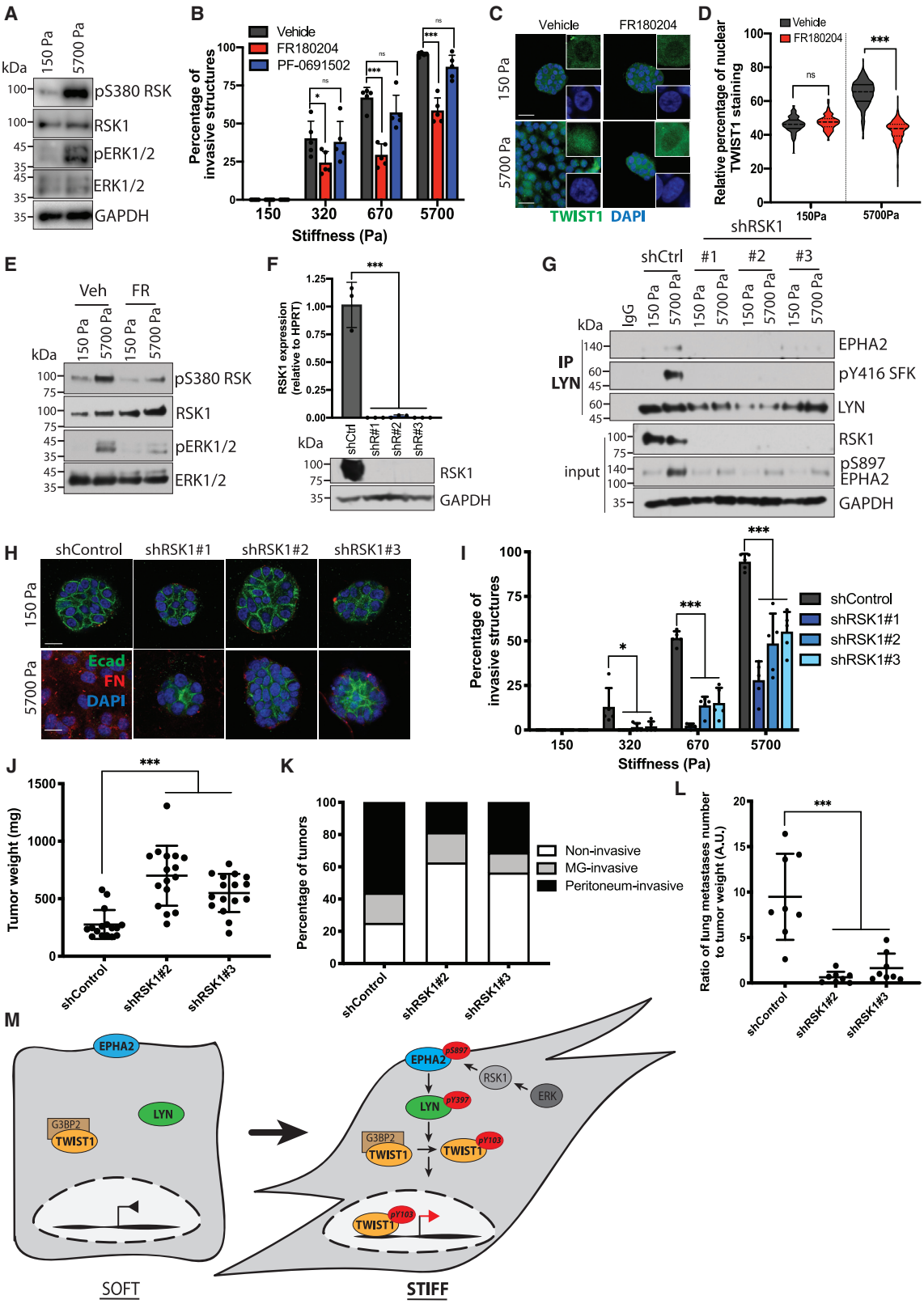

(legend on next page)

CA030199 and Sanford Burnham Prebys Institutional funding to E.B.P., and grant PTC2017 from Padres Pedal the Cause to J.Y. and E.B.P.; L.F. was supported by an AACR Basic Cancer Research fellowship.

AUTHOR CONTRIBUTIONS

Conceptualization, L.F. and J.Y.; Methodology, L.F., J.Y., and E.B.P.; Investigation, L.F., H.-Y.J., M.W.M., B.E.A., A.K., and A.C.C.; Writing – Original Draft, L.F.; Writing – Review & Editing, L.F., J.Y., and E.B.P.; Funding Acquisition, L.F., J.Y., and E.B.P.; Resources, A.C.C., R.L.S., A.K., and A.J.E.; Supervision, J.Y. and E.B.P.

DECLARATION OF INTERESTS

The authors declare no competing interests.

Received: October 28, 2019
Revised: April 15, 2020
Accepted: May 28, 2020
Published: June 22, 2020

REFERENCES

Barquilla, A., Lamberto, I., Noberini, R., Heynen-Genel, S., Brill, L.M., and Pasquale, E.B. (2016). Protein kinase A can block EphA2 receptor-mediated cell repulsion by increasing EphA2 S897 phosphorylation. Mol. Biol. Cell *27*, 2757–2770.

Barriga, E.H., Franze, K., Charras, G., and Mayor, R. (2018). Tissue stiffening coordinates morphogenesis by triggering collective cell migration in vivo. Nature *554*, 523–527.

Boyd, N.F., Dite, G.S., Stone, J., Gunasekara, A., English, D.R., McCredie, M.R., Giles, G.G., Tritchler, D., Chiarelli, A., Yaffe, M.J., and Hopper, J.L. (2002). Heritability of mammographic density, a risk factor for breast cancer. N. Engl. J. Med. *347*, 886–894.

Brabletz, T., Kalluri, R., Nieto, M.A., and Weinberg, R.A. (2018). EMT in cancer. Nat. Rev. Cancer *18*, 128–134.

Brantley-Sieders, D.M., and Chen, J. (2004). Eph receptor tyrosine kinases in angiogenesis: from development to disease. Angiogenesis *7*, 17–28.

Broders-Bondon, F., Nguyen Ho-Bouldoires, T.H., Fernandez-Sanchez, M.E., and Farge, E. (2018). Mechanotransduction in tumor progression: the dark side of the force. J. Cell Biol. *217*, 1571–1587.

Cartwright, C.A., Eckhart, W., Simon, S., and Kaplan, P.L. (1987). Cell transformation by pp60c-src mutated in the carboxy-terminal regulatory domain. Cell *49*, 83–91.

Chang, J.M., Park, I.A., Lee, S.H., Kim, W.H., Bae, M.S., Koo, H.R., Yi, A., Kim, S.J., Cho, N., and Moon, W.K. (2013). Stiffness of tumours measured by shear-wave elastography correlated with subtypes of breast cancer. Eur. Radiol. *23*, 2450–2458.

Chaudhuri, T., Rehfeldt, F., Sweeney, H.L., and Discher, D.E. (2010). Preparation of collagen-coated gels that maximize in vitro myogenesis of stem cells by matching the lateral elasticity of in vivo muscle. Methods Mol. Biol. *621*, 185–202.

Choi, Y.L., Bocanegra, M., Kwon, M.J., Shin, Y.K., Nam, S.J., Yang, J.H., Kao, J., Godwin, A.K., and Pollack, J.R. (2010). LYN is a mediator of epithelial-mesenchymal transition and a target of dasatinib in breast cancer. Cancer Res. *70*, 2296–2306.

Colpaert, C., Vermeulen, P., Van Marck, E., and Dirix, L. (2001). The presence of a fibrotic focus is an independent predictor of early metastasis in lymph node-negative breast cancer patients. Am. J. Surg. Pathol. *25*, 1557–1558.

Debnath, J., Muthuswamy, S.K., and Brugge, J.S. (2003). Morphogenesis and oncogenesis of MCF-10A mammary epithelial acini grown in three-dimensional basement membrane cultures. Methods *30*, 256–268.

Dupont, S., Morsut, L., Aragona, M., Enzo, E., Giulitti, S., Cordenonsi, M., Zanconato, F., Le Digabel, J., Forcato, M., Bicciato, S., et al. (2011). Role of YAP/TAZ in mechanotransduction. Nature *474*, 179–183.

Eckert, M.A., Lwin, T.M., Chang, A.T., Kim, J., Danis, E., Ohno-Machado, L., and Yang, J. (2011). Twist1-induced invadopodia formation promotes tumor metastasis. Cancer Cell *19*, 372–386.

Hasebe, T., Sasaki, S., Imoto, S., Mukai, K., Yokose, T., and Ochiai, A. (2002). Prognostic significance of fibrotic focus in invasive ductal carcinoma of the breast: a prospective observational study. Mod. Pathol. *15*, 502–516.

Johnson, K.R., Leight, J.L., and Weaver, V.M. (2007). Demystifying the effects of a three-dimensional microenvironment in tissue morphogenesis. Methods Cell Biol. *83*, 547–583.

Klenova, E., Chernukhin, I., Inoue, T., Shamsuddin, S., and Norton, J. (2002). Immunoprecipitation techniques for the analysis of transcription factor complexes. Methods *26*, 254–259.

Kmiecik, T.E., and Shalloway, D. (1987). Activation and suppression of pp60c-src transforming ability by mutation of its primary sites of tyrosine phosphorylation. Cell *49*, 65–73.

Laklai, H., Miroshnikova, Y.A., Pickup, M.W., Collisson, E.A., Kim, G.E., Barrett, A.S., Hill, R.C., Lakins, J.N., Schlaepfer, D.D., Mouw, J.K., et al. (2016). Genotype tunes pancreatic ductal adenocarcinoma tissue tension to induce matricellular fibrosis and tumor progression. Nat. Med. *22*, 497–505.

Figure 6. ERK/RSK1-Dependent EPHA2 Phosphorylation on S897 Is Required for LYN Activation and Cell Invasion in Response to ECM Stiffness

(A) Lysates from 3D-cultured MCF10A cells were immunoblotted as indicated.

(B–D) MCF10A cells were grown on 3D-PA gels for 5 days in presence of 5 μM ERK1/2 inhibitor (FR180204), 100 nM AKT inhibitor (PF-0691502), or vehicle control (DMSO). (B) Cell phenotypes were quantified as percentage of invasive structures. Data are presented as mean ± SD, dots represent individual fields. (C) Cells were stained for TWIST1 (green) and DAPI (blue). Scale bar represents 25 μm. Inserts show high-magnification images. (D) TWIST1 nuclear signal in (C) is presented as percentage of total TWIST1 staining on a violin plot showing the distribution of the data with the median (hyphen line) and quartiles (dotted line).

(E) Lysates from 3D-cultured MCF10A cells treated for 2 h with 5 μM ERK1/2 inhibitor (FR) or vehicle control (DMSO) were immunoblotted as indicated.

(F) Upper panel, qPCR analysis in MCF10A cells. Data are presented as mean ± SD, dots represent technical replicates. Lower panel, WBs in lysate from MCF10A cells as indicated.

(G–I) Control or RSK1-silenced MCF10A cells were grown on 3D-PA gels for 5 days. (G) Lysates were subjected to LYN immunoprecipitation and immunoblotted as indicated. (H) Cells were stained for E-cadherin (green), DAPI (blue), and FN (red). Scale bar represents 25 μm. (I) Cell phenotypes were quantified as percentage of invasive structures. Data are presented as mean ± SD, dots represent individual fields.

(J) GFP-labeled control or RSK1-silenced MCF10DCIS cells injected into the mammary gland of NOD/SCID mice. Tumor weight (mg) at the end of the experiment are presented as mean ± SD, dots represent individual tumors. n = 16 tumors per group.

(K) Regional (peritoneum) invasion of the primary tumors presented as percentage of total primary tumors. N = 8 mice per group.

(L) Lung metastatic burden presented as the ratio of the number of GFP+ nodules in the lungs to tumor weight. a.u., arbitrary units. Data are presented as mean ± SD, dots represent individual animals. N = 8 mice per group.

(M) Schematic model of the mechanosensitive activation of EPHA2, LYN, and TWIST1.

***$p < 0.001$; *$p < 0.05$; ns, not significant.

See also Figure S6.

Please cite this article in press as: Fattet et al., Matrix Rigidity Controls Epithelial-Mesenchymal Plasticity and Tumor Metastasis via a Mechanoresponsive EPHA2/LYN Complex, Developmental Cell (2020), https://doi.org/10.1016/j.devcel.2020.05.031

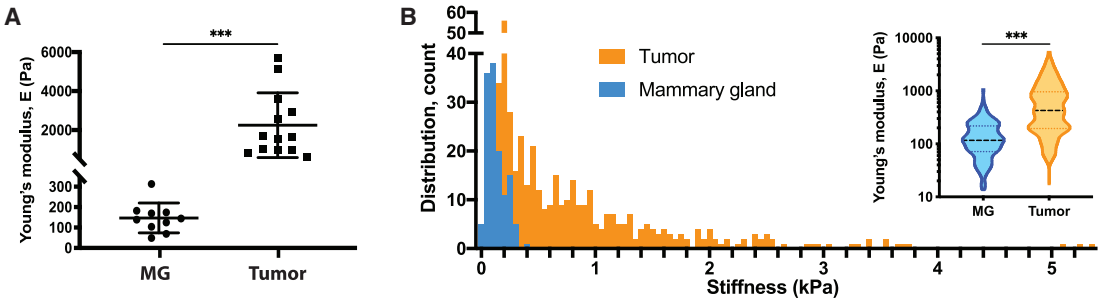

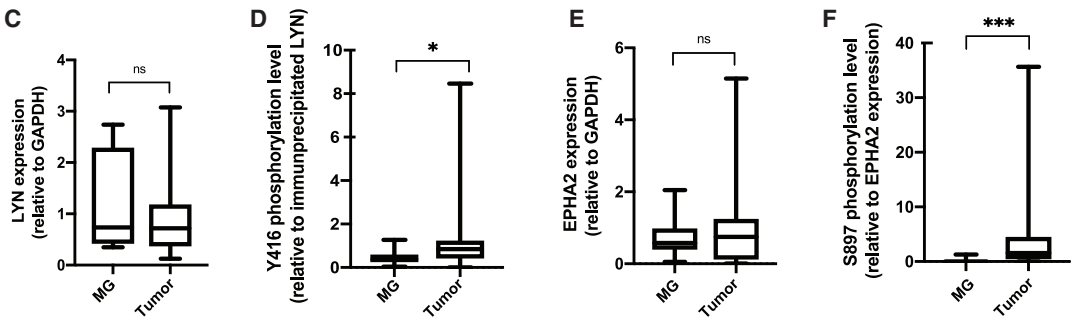

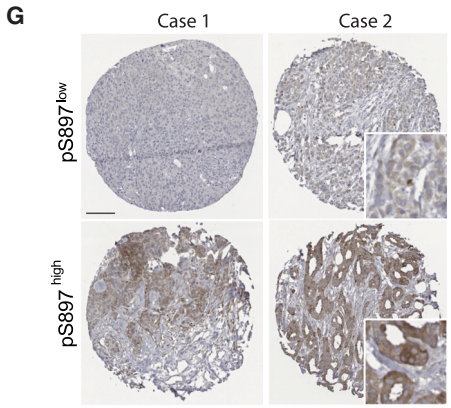

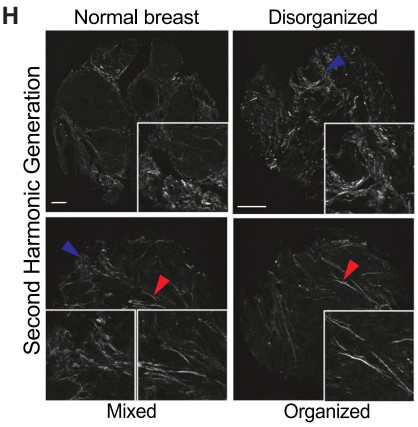

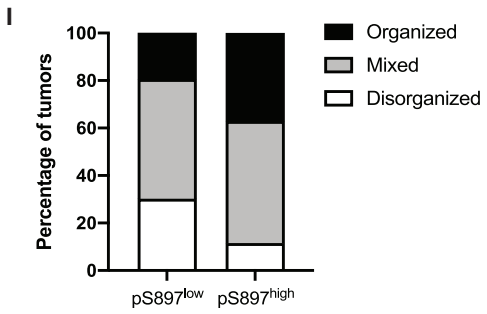

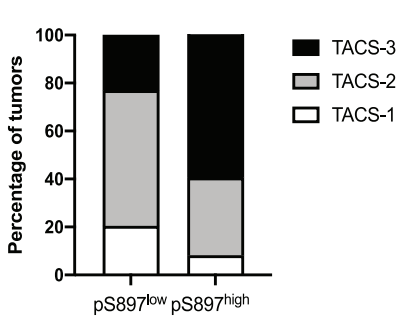

J

	Disorganized	Mixed	Organized
pS897^{low}	34 (29.01)	57 (57.26)	22 (26.72)
pS897^{high}	4 (8.99)	18 (17.74)	13 (8.28)

$X^2 = 7.1588$
$p = 0.0279$

L

	TACS-1	TACS-2	TACS-3
pS897^{low}	23 (19.59)	64 (57.25)	26 (36.16)
pS897^{high}	3 (6.41)	12 (18.75)	22 (11.84)

$X^2 = 17.2076$
$p = 0.0002$

Figure 7. Activation of EPHA2 Non-canonical Signaling Correlates with Matrix Stiffening during Breast Tumor Progression and Metastasis

(A) Rheology measurements of normal mammary glands (MG) and tumors from MCF10DCIS xenografts. Data are presented as mean ± SD, dots represent individual samples. N = 10 (MG) and 13 (tumors).

(legend continued on next page)

Levental, K.R., Yu, H., Kass, L., Lakins, J.N., Egeblad, M., Erler, J.T., Fong, S.F., Csiszar, K., Giaccia, A., Weninger, W., et al. (2009). Matrix crosslinking forces tumor progression by enhancing integrin signaling. Cell *139*, 891–906.

Li, J.Y., Xiao, T., Yi, H.M., Yi, H., Feng, J., Zhu, J.F., Huang, W., Lu, S.S., Zhou, Y.H., Li, X.H., and Xiao, Z.-Q. (2019). S897 phosphorylation of EphA2 is indispensable for EphA2-dependent nasopharyngeal carcinoma cell invasion, metastasis and stem properties. Cancer Lett. *444*, 162–174.

Lu, P., Weaver, V.M., and Werb, Z. (2012). The extracellular matrix: a dynamic niche in cancer progression. J. Cell Biol. *196*, 395–406.

Majeski, H.E., and Yang, J. (2016). The 2016 John J. Abel award lecture: targeting the mechanical microenvironment in cancer. Mol. Pharmacol. *90*, 744–754.

Martino, F., Perestrelo, A.R., Vinarský, V., Pagliari, S., and Forte, G. (2018). Cellular mechanotransduction: from tension to function. Front. Physiol. *9*, 824.

Miao, H., Li, D.Q., Mukherjee, A., Guo, H., Petty, A., Cutter, J., Basilion, J.P., Sedor, J., Wu, J., Danielpour, D., et al. (2009). EphA2 mediates ligand-dependent inhibition and ligand-independent promotion of cell migration and invasion via a reciprocal regulatory loop with Akt. Cancer Cell *16*, 9–20.

Miller, F.R., Santner, S.J., Tait, L., and Dawson, P.J. (2000). MCF10DCIS.com xenograft model of human comedo ductal carcinoma in situ. J. Natl. Cancer Inst. *92*, 1185–1186.

Miroshnikova, Y.A., Mouw, J.K., Barnes, J.M., Pickup, M.W., Lakins, J.N., Kim, Y., Lobo, K., Persson, A.I., Reis, G.F., McKnight, T.R., et al. (2016). Tissue mechanics promote IDH1-dependent HIF1alpha-tenascin C feedback to regulate glioblastoma aggression. Nat. Cell Biol. *18*, 1336–1345.

Mujtaba, S.S., Ni, Y.B., Tsang, J.Y., Chan, S.K., Yamaguchi, R., Tanaka, M., Tan, P.H., and Tse, G.M. (2013). Fibrotic focus in breast carcinomas: relationship with prognostic parameters and biomarkers. Ann. Surg. Oncol. *20*, 2842–2849.

Paraiso, K.H., Das Thakur, M., Fang, B., Koomen, J.M., Fedorenko, I.V., John, J.K., Tsao, H., Flaherty, K.T., Sondak, V.K., Messina, J.L., et al. (2015). Ligand-independent EPHA2 signaling drives the adoption of a targeted therapy-mediated metastatic melanoma phenotype. Cancer Discov. *5*, 264–273.

Park, C.C., Zhang, H., Pallavicini, M., Gray, J.W., Baehner, F., Park, C.J., and Bissell, M.J. (2006). Beta1 integrin inhibitory antibody induces apoptosis of breast cancer cells, inhibits growth, and distinguishes malignant from normal phenotype in three dimensional cultures and in vivo. Cancer Res. *66*, 1526–1535.

Pasquale, E.B. (2008). Eph-ephrin bidirectional signaling in physiology and disease. Cell *133*, 38–52.

Pasquale, E.B. (2010). Eph receptors and ephrins in cancer: bidirectional signalling and beyond. Nat. Rev. Cancer *10*, 165–180.

Paszek, M.J., Zahir, N., Johnson, K.R., Lakins, J.N., Rozenberg, G.I., Gefen, A., Reinhart-King, C.A., Margulies, S.S., Dembo, M., Boettiger, D., et al. (2005). Tensional homeostasis and the malignant phenotype. Cancer Cell *8*, 241–254.

Provenzano, P.P., Eliceiri, K.W., Campbell, J.M., Inman, D.R., White, J.G., and Keely, P.J. (2006). Collagen reorganization at the tumor-stromal interface facilitates local invasion. BMC Med. *4*, 38.

Rohani, N., Canty, L., Luu, O., Fagotto, F., and Winklbauer, R. (2011). EphrinB/EphB signaling controls embryonic germ layer separation by contact-induced cell detachment. PLoS Biol. *9*, e1000597.

Smith, A., Robinson, V., Patel, K., and Wilkinson, D.G. (1997). The EphA4 and EphB1 receptor tyrosine kinases and ephrin-B2 ligand regulate targeted migration of branchial neural crest cells. Curr. Biol. *7*, 561–570.

Tabariès, S., Annis, M.G., Hsu, B.E., Tam, C.E., Savage, P., Park, M., and Siegel, P.M. (2015). Lyn modulates Claudin-2 expression and is a therapeutic target for breast cancer liver metastasis. Oncotarget *6*, 9476–9487.

Thaper, D., Vahid, S., Nip, K.M., Moskalev, I., Shan, X., Frees, S., Roberts, M.E., Ketola, K., Harder, K.W., Gregory-Evans, C., et al. (2017). Targeting Lyn regulates Snail family shuttling and inhibits metastasis. Oncogene *36*, 3964–3975.

Thomas, S.M., and Brugge, J.S. (1997). Cellular functions regulated by Src family kinases. Annu. Rev. Cell Dev. Biol. *13*, 513–609.

Tornillo, G., Knowlson, C., Kendrick, H., Cooke, J., Mirza, H., Aurrekoetxea-Rodríguez, I., Vivanco, M.D.M., Buckley, N.E., Grigoriadis, A., and Smalley, M.J. (2018). Dual mechanisms of LYN kinase dysregulation drive aggressive behavior in breast cancer cells. Cell Rep. *25*, 3674–3692.e10.

Tsai, J.H., Donaher, J.L., Murphy, D.A., Chau, S., and Yang, J. (2012). Spatiotemporal regulation of epithelial-mesenchymal transition is essential for squamous cell carcinoma metastasis. Cancer Cell *22*, 725–736.

Wei, S.C., Fattet, L., Tsai, J.H., Guo, Y., Pai, V.H., Majeski, H.E., Chen, A.C., Sah, R.L., Taylor, S.S., Engler, A.J., and Yang, J. (2015). Matrix stiffness drives epithelial-mesenchymal transition and tumour metastasis through a TWIST1-G3BP2 mechanotransduction pathway. Nat. Cell Biol. *17*, 678–688.

Yang, B., Lieu, Z.Z., Wolfenson, H., Hameed, F.M., Bershadsky, A.D., and Sheetz, M.P. (2016). Mechanosensing controlled directly by tyrosine kinases. Nano Lett. *16*, 5951–5961.

Yang, J., Mani, S.A., Donaher, J.L., Ramaswamy, S., Itzykson, R.A., Come, C., Savagner, P., Gitelman, I., Richardson, A., and Weinberg, R.A. (2004). Twist, a master regulator of morphogenesis, plays an essential role in tumor metastasis. Cell *117*, 927–939.

Zelinski, D.P., Zantek, N.D., Stewart, J.C., Irizarry, A.R., and Kinch, M.S. (2001). EphA2 overexpression causes tumorigenesis of mammary epithelial cells. Cancer Res. *61*, 2301–2306.

Zhao, B., Wei, X., Li, W., Udan, R.S., Yang, Q., Kim, J., Xie, J., Ikenoue, T., Yu, J., Li, L., et al. (2007). Inactivation of YAP oncoprotein by the Hippo pathway is involved in cell contact inhibition and tissue growth control. Genes Dev. *21*, 2747–2761.

Zhou, Y., and Sakurai, H. (2017). Emerging and diverse functions of the EphA2 noncanonical pathway in cancer progression. Biol. Pharm. Bull. *40*, 1616–1624.

Zhou, Y., Yamada, N., Tanaka, T., Hori, T., Yokoyama, S., Hayakawa, Y., Yano, S., Fukuoka, J., Koizumi, K., Saiki, I., and Sakurai, H. (2015). Crucial roles of RSK in cell motility by catalysing serine phosphorylation of EphA2. Nat. Commun. *6*, 7679.

(B) Atomic force microscopy measurements of normal MG and tumors from MCF10DCIS xenografts. Each bar represents the distribution of samples in a 50 Pa-range. Insert: violin plot depicting the mean Young's modulus E (Pa).
(C–F) Normal MG and tumors from MCF10DCIS xenografts were processed for protein extraction. (C) Lysates were immunoblotted for LYN and GAPDH, protein amounts were quantified by densitometry (presented as the ratio of LYN to GAPDH expression). (D) Lysates were subjected to LYN immunoprecipitation and immunoblotted for phospho-Y416 SFK. Phosphorylation levels were quantified (presented as the ratio of phospho-Y416 to total LYN expression). (E) Lysates were immunoblotted for EPHA2 and protein amounts were quantified (presented as the ratio of EPHA2 to GAPDH expression). (F) Lysates were immunoblotted for phospho-S897 EPHA2. Phosphorylation levels were quantified by densitometry (presented as the ratio of phospho-S897 to EPHA2 expression).
(G) IHC for phospho-S897 EPHA2. Scale bar represents 50 μm. Inserts show higher magnification.
(H) SHG imaging. Scale bar represents 50 μm. Inserts show higher magnification. Red arrows show straight collagen fibers (organized), blue arrows show curved collagen (disorganized).
(I and J) Correlation analysis between collagen organization (SHG) and phospho-S897 EPHA2 (IHC) staining. (I) Bar graph showing the repartition of breast tumors. (J) χ^2 analysis showing that collagen organization and phospho-S897 EPHA2 status are correlated.
(K and L) Correlation analysis between TACS score (SHG) and phospho-S897 EPHA2 (IHC) staining. (K) Bar graph showing the repartition of breast tumors. (L) χ^2 analysis showing that TACS score and phospho-S897 EPHA2 status are correlated.
***$p < 0.001$; *$p < 0.05$; ns, not significant.
See also Figure S7.

Please cite this article in press as: Fattet et al., Matrix Rigidity Controls Epithelial-Mesenchymal Plasticity and Tumor Metastasis via a Mechanoresponsive EPHA2/LYN Complex, Developmental Cell (2020), https://doi.org/10.1016/j.devcel.2020.05.031

STAR★METHODS

KEY RESOURCES TABLE

REAGENT or RESOURCE	SOURCE	IDENTIFIER
Antibodies		
G3BP2	Sigma-Aldrich	Cat#HPA018304; RRID: AB_1849350
TWIST1	Santa Cruz Biotechnology	Cat#81417; RRID: AB_1130910
TWIST1	Hybridoma	Clone 5b7
pY103 Twist1	Abgent	Cat#AP22382a
EPHA2	Cell Signaling Technology	Cat#6997; RRID: AB_10827743
EPHA1	R&D Systems	Cat#AF638; RRID: AB_2098926
EPHA4	ThermoFisher	Cat#37-1600; RRID: AB_2533301
EphrinA1	Abcam	Cat# 124911; RRID: AB_10974078
LYN	Cell Signaling Technology	Cat#2796; RRID: AB_2138391
FRK	Assay Biotechnology	Cat#C10609; RRID: AB_10685478
Myc	Hybridoma	Clone 9E10
Myc	Cell Signaling Technology	Cat#2276; RRID: AB_331783
pY416 SFK	Cell Signaling Technology	Cat#2101; RRID: AB_331697
pY527 SFK	Cell Signaling Technology	Cat#2105; RRID: AB_331034
SRC	Cell Signaling Technology	Cat#2109; RRID: AB_2106059
GAPDH	Genetex	Cat#GTX100118; RRID: AB_1080976
GFP	Abcam	Cat#Ab13970; RRID: AB_300798
Flag	Sigma Aldrich	Cat#F3165; RRID: AB_259529
Flag	Cell Signaling Technology	Cat#14793; RRID: AB_2572291
pY397 FAK	Cell Signaling Technology	Cat#8556; RRID: AB_10891442
RSK1	Cell Signaling Technology	Cat#9333; RRID: AB_2181177
pRSK (pS380)	Cell Signaling Technology	Cat#9335; RRID: AB_561151
AKT	Cell Signaling Technology	Cat#9272; RRID: AB_329827
pAKT (pT308)	Cell Signaling Technology	Cat#9275; RRID: AB_329828
ERK1/2	Cell Signaling Technology	Cat#4695; RRID: AB_390779
pERK1/2 (pT202/Y204)	Cell Signaling Technology	Cat#4370; RRID: AB_2315112

(*Continued on next page*)

Please cite this article in press as: Fattet et al., Matrix Rigidity Controls Epithelial-Mesenchymal Plasticity and Tumor Metastasis via a Mechanoresponsive EPHA2/LYN Complex, Developmental Cell (2020), https://doi.org/10.1016/j.devcel.2020.05.031

Continued

REAGENT or RESOURCE	SOURCE	IDENTIFIER
Integrin β1	Santa Cruz Biotechnology	Cat#374430; RRID: AB_10991321
Mouse IgG control (IP)	Santa Cruz Biotechnology	Cat#2025; RRID: AB_737182
Rabbit IgG control (IP)	Cell Signaling Technology	Cat#2729; RRID: AB_1031062
pS897 EPHA2	Cell Signaling Technology	Cat#6347; RRID: AB_11220420
pY588 EPHA2	Cell Signaling Technology	Cat#12677; RRID: AB_2797989
Goat anti-Mouse-HPR	Jackson Immunoresearch	Cat#115-035-003; RRID: AB_10015289
Goat anti-Rabbit-HPR	Jackson Immunoresearch	Cat#111-035-144; RRID: AB_2307391
Bovine anti-Goat-HPR	Jackson Immunoresearch	Cat#805-035-180; RRID: AB_2340874
Goat anti-Mouse Alexa Fluor 488	Invitrogen	Cat#A-11001; RRID: AB_2534069
Goat anti-Rabbit Alexa Fluor 546	Invitrogen	Cat#A-11010; RRID: AB_2534077
Biological Samples		
CDP Breast Cancer Stage III Prognostic TMA	NCI	N/A
Chemicals, Peptides, and Recombinant Proteins		
Recombinant active LYN	Sigma Aldrich	Cat#SRP5277
Recombinant ephrinA1-Fc	R&D Systems	Cat#602-A1-200
Bafetinib	Selleckchem	Cat#S1369
Nilotinib	Selleckchem	Cat#S1033
BI-D1870	Selleckchem	Cat#S2843
PP2	Selleckchem	Cat#S7008
VS-4718	Schlaepfer lab (UCSD)	N/A
FR180204	Burgoyne lab (UCSD)	N/A
PF-0691502	Burgoyne lab (UCSD)	N/A
Critical Commercial Assays		
Duolink Proximity Ligation Assay	Sigma Aldrich	Cat#DUO92007
Accustain Trichrome Satin kit	Sigma Aldrich	Cat#HT15
Experimental Models: Cell Lines		
MCF10A	ATCC	Cat#CRL-10317; RRID: CVCL_0598
MCF10DCIS	Miller lab	Miller et al., 2000; RRID: CVCL_5552
EpH4Ras	Reichmann lab (Zurich)	N/A
293T	ATCC	Cat#ACS-4500; RRID: CVCL_0063
293AD	Agilent Technologies	Cat#240085; RRID: CVCL_KA63
Experimental Models: Organisms/Strains		
Mouse: CB17.Cg-Prkdc^{scid}Lyst^{bg-J}/Crl	Charles River	Cat#250; RRID: IMSR_CRL:250
Oligonucleotides		
Primers for qPCR	Designed using PrimerBank	See Table S1

(*Continued on next page*)

Please cite this article in press as: Fattet et al., Matrix Rigidity Controls Epithelial-Mesenchymal Plasticity and Tumor Metastasis via a Mechanoresponsive EPHA2/LYN Complex, Developmental Cell (2020), https://doi.org/10.1016/j.devcel.2020.05.031

Continued

REAGENT or RESOURCE	SOURCE	IDENTIFIER
shRNA Sequences	Sigma Aldrich	See Table S2
Recombinant DNA		
pcDNA4B-Myc-His_6-TWIST1 WT and Y107F	This paper	N/A
pLV-Puro-LYN WT and Y508F	Vectorbuilder	Custom order
pEGFP-C1-G3BP2	Dargemont lab (Paris)	N/A
pLVX-IRES-Neo	Clontech	Cat#632181
pKH-RSK1	Taylor lab (UCSD)	N/A
pWB-RSK1 WT and K94R/K447R	This paper	N/A
Software and Algorithms		
ImageJ	NIH	https://imagej.nih.gov/ij/
PRISM	Graphpad	N/A
CurveAlign	LOCI	https://loci.wisc.edu/software/curvealign

RESOURCE AVAILABILITY

Lead Contact

Further information and requests for resources and reagents should be directed to and will be fulfilled by the Lead Contact, Jing Yang (jingyang@ucsd.edu).

Materials Availability

All unique/stable reagents generated in this study are available from the Lead Contact with a completed Materials Transfer Agreement.

Data and Code Availability

This study did not generate/analyse datasets/codes.

EXPERIMENTAL MODEL AND SUBJECT DETAILS

Cell Lines

MCF10A and 293T cells were purchased from the ATCC. 293AD cells were purchased from Agilent Technologies. MCF10DCIS cells were obtained from the Miller laboratory (Wayne State University, Detroit). Eph4Ras cells were obtained from the Reichmann laboratory (Zurich, Switzerland).

Mouse Strain

For xenograft tumor assay, 6 to 8-week-old female SCID-beige mice CB17.Cg-Prkdc^{scid}Lyst^{bg-J}/Crl were purchased from Charles River.

METHOD DETAILS

Cell Culture

MCF10A and MCF10DCIS cells were grown in DMEM/F12 media supplemented with 5% horse serum, 20 ng/ml human EGF (hEGF), 10 μg/ml insulin, 0.5 μg/ml hydrocortisone, 1% penicillin and streptomycin, and 100ng/ml cholera toxin. Eph4Ras cells were cultured as previously described in MEGM mixed 1:1 with DMEM/F12 media supplemented with 10ng/ml hEGF, 10 μg/ml insulin, 0.5 μg/ml hydrocortisone, 1% penicillin and streptomycin (Eckert et al., 2011). 293T and 293AD cells were cultured in DMEM media supplemented with 10% foetal bovine serum (FBS) and 1% penicillin and streptomycin. All cell lines were tested negative for mycoplasma contamination.

DNA Constructs

For His-tag purification using Ni-NTA beads, TWIST1 was cloned into the pcDNA4B-Myc-His_6. pLV-Puro-LYN WT and pLV-Puro-LYN Y508F were custom ordered from Vectorbuilder. pEGFP-C1-G3BP2 construct was kindly provided by C. Dargemont (Institut Curie, Paris, France). We generated pLVX-IRES-Neo (Clontech, # 632181) constructs encoding EPHA2 with the Strep-tag II sequence (WSHPQFEK) at the N-terminus, which in some constructs was preceded by a FLAG tag sequence. As a control, we

Please cite this article in press as: Fattet et al., Matrix Rigidity Controls Epithelial-Mesenchymal Plasticity and Tumor Metastasis via a Mechanoresponsive EPHA2/LYN Complex, Developmental Cell (2020), https://doi.org/10.1016/j.devcel.2020.05.031

used a construct encoding EPHA2 wild-type with only an N-terminal FLAG sequence (Barquilla et al., 2016). In addition, we generated LYN constructs encoding LYN with a C-terminal Myc tag in pLV-Puro (Vectorbuilder) to distinguish introduced LYN from endogenously expressed LYN. The pKH-RSK1 construct was kindly provided by Prof. S. Taylor (UCSD). The RSK1 cDNA was subcloned into the retroviral pWB backbone and the kinase dead (KD) RSK1 was obtained by double mutation of K94R and K447R. Tagged constructs and mutants were obtained by site-directed mutagenesis using the QuikChange II kit (Agilent) or by overlapping PCR.

Generation of Stable Cell Lines

Stable gene knockdown cell lines were generated using lentiviral or retroviral plasmid vectors. Briefly, 293T cells were transfected with pCMVΔ8.2R (for lentivirus) or pUMVC3 (for retrovirus), VSVG and the pLKO.1 construct containing the shRNA of interest, pLV lentiviral construct expressing LYN or EPHA2 or pWB retroviral construct expressing RSK1 (ratio 2:1:10). Viral supernatants were then concentrated using Lenti-X^{TM} concentrator (Takara). Concentrated viral supernatants were applied to target cells with 6 μg/ml protamine sulfate. Infection was repeated the next day. Infected cells were then selected with puromycin (2 μg/ml), G418 (400 μg/ml) or Blasticidin (5 μg/ml).

Polyacrylamide Hydrogel Preparation

Hydrogels were prepared as previously described on 12 mm and 25 mm coverslips (Chaudhuri et al., 2010). Briefly, No. 1 glass coverslips were etched using UV/Ozone Procleaner Plus, functionalized using 3-Aminopropyltriethoxysilane, rinsed with dH_2O, incubated in 0.5% gluteraldehyde in PBS, dried, and then acrylamide/bis-acrylamide mixtures were polymerized between the functionalized coverslip and a glass slide coated with dichlorodimethylsiloxane. Polyacrylamide coated coverslips were then washed twice with dH_2O, incubated with 1mM Sulfo-SANPAH in HEPES buffer under 365nm UV light for 10 minutes, rinsed twice with 50mM HEPES pH 8.5 buffer, incubated at 37°C overnight with rat tail Collagen I (Millipore) in 50mM HEPES pH 8.5 buffer, rinsed twice in PBS, and sterilized. For IP-LC-MS/MS experiments, custom-made easy-coat 100mm Petrisoft dishes were purchased from Matrigen (La Brea, CA, USA).

3-dimensional (3D) Cell Culture

MCF10A and Eph4Ras cells were grown in 3D cell culture as previously described (Debnath et al., 2003). Briefly, Eph4Ras cells were seeded on top of collagen-coated hydrogels in 2% Matrigel-MEGM mixed 1:1 with DMEM/F12 and MCF10A cells were seeded similarly in DMEM/F12 medium supplemented with 2% horse serum, 5 ng/ml human EGF, 10 μg/ml insulin, 0.5 μg/ml hydrocortisone, penicillin, streptomycin, and 100 ng/ml cholera toxin.

3D Confocal Microscopy

Our protocol was adapted from the method described by Debnath et al (Debnath et al., 2003). Briefly, cells were fixed with 2% paraformaldehyde (PFA) for 20 minutes at room temperature, permeabilized with PBS-0.5% Triton X-100 for 10 minutes, quenched with 3 washes of 100mM PBS-glycine, and then blocked with 20% goat serum in immunofluorescence (IF) buffer. Samples were incubated with primary antibodies overnight in 20% goat serum-IF buffer, washed 3 times with IF buffer, incubated with secondary antibodies (1:200 dilution) for 1 hour at room temperature, and mounted in DAPI-containing mounting medium (Vector Laboratories). Confocal images were acquired using an Olympus FV1000 with 405, 488, 555, and 647 laser lines. Images were linearly analysed and pseudocoloured using ImageJ analysis software.

Second Harmonic Generation Microscopy

An SP8 resonant laser-scanning confocal system mounted on a DM 6000 upright microscope (Leica Microsystems) with a 10X or 25X air objective, 0.4 NA was used for second-harmonic generation microscopy. A Ti-Sapphire femtosecond pulsed Chameleon Ultra II (Coherent Inc.) laser was tuned to 855 nm and the emitted fluorescent signal was recorded with a non-descanned hybrid detector fitted with a 425/26 nm bandpass filter. To increase the signal to noise ratio, 1248x1248 pixel 8-bit images (0.6 μm/pixel) were acquired with 16x line averaging and 8 frames image accumulation. Images were exported as TIFF files and analysed with CT-FIRE module from the CurveAlign software.

Tumor Tissue Microarrays

Stage 3 breast cancer progression tumor tissue microarrays (TMAs) from the National Cancer Institute Cancer Diagnosis Program were stained for phospho-Ser897 EPHA2 by immunohistochemistry for retrospective analysis. TMAs were concurrently scanned using the NanoZoomer Slide Scanner with a 10X objective and imaged by SHG.

Immunoprecipitation

Cells were lysed using a 2-step protocol adapted from Klenova et al (Klenova et al., 2002). Cells were directly lysed with lysis buffer (20mM Tris-HCl, 1% Triton X-100, 10mM $MgCl_2$, 10mM KCl, 2mM EDTA, 1mM NaF, 1mM sodium orthovanadate, 2.5mM beta-glycerophosphate, 10% glycerol, pH 7.5), scraped off the culture dish, sonicated, supplemented to 400mM NaCl, sonicated, and diluted to 200mM NaCl. Lysates were precleared with protein G beads for 1 hour at 4°C. Antibodies were conjugated to protein G beads (Invitrogen), crosslinked using disuccinimidyl suberate (Pierce) as per manufacturer's protocol, incubated with lysates overnight at 4°C, washed eight times with IP lysis buffer supplemented with 200 mM NaCl, and eluted by incubation LDS sample buffer with

Please cite this article in press as: Fattet et al., Matrix Rigidity Controls Epithelial-Mesenchymal Plasticity and Tumor Metastasis via a Mechanoresponsive EPHA2/LYN Complex, Developmental Cell (2020), https://doi.org/10.1016/j.devcel.2020.05.031

50 mM DTT at 70°C for 15 minutes. 5B7 mouse hybridoma concentrated supernatant was used for endogenous TWIST1 immunoprecipitation. For immunoprecipitation of exogenously transfected Myc-TWIST1, 293T cell lysates were harvested 48 hours after transfection and subjected to the 2-step lysis protocol. Immunoprecipitation was performed using anti-Myc antibody (9E10) cross-linked to protein A agarose beads (Invitrogen).

Mass Spectrometry

After immunoprecipitation and washing, beads were washed 3 times with PBS and snap-frozen before being subjected to on-bead digestion. Trypsin-digested peptides were analysed by ultra-high-pressure liquid chromatography (UPLC) coupled with tandem mass spectroscopy (LC-MS/MS) using nanospray ionization. The nanospray ionization experiments were performed using an Orbitrap fusion Lumos hybrid mass spectrometer (Thermo) interfaced with nanoscale reversed-phase UPLC (Thermo Dionex UltiMate™ 3000 RSLC nano System) using a 25 cm, 75-micron ID glass capillary packed with 1.7-μm C18 (130) BEH™ beads (Waters corporation). Peptides were eluted from the C18 column into the mass spectrometer using a linear gradient (5–80%) of ACN (Acetonitrile) at a flow rate of 375 μl/min for 1h. The buffers used to create the ACN gradient were: Buffer A (98% H_2O, 2% ACN, 0.1% formic acid) and Buffer B (100% ACN, 0.1% formic acid). Mass spectrometer parameters are as follows; an MS1 survey scan using the orbitrap detector (mass range (m/z): 400-1500 (using quadrupole isolation), 60000 resolution setting, spray voltage of 2400 V, Ion transfer tube temperature of 285 C, AGC target of 400000, and maximum injection time of 50 ms was followed by data dependent scans (top speed for most intense ions, with charge state set to only include +2-5 ions, and 5 second exclusion time, while selecting ions with minimal intensities of 50000 at in which the collision event was carried out in A- high energy collision cell (HCD Collision Energy of 30%), and the fragment masses where analysed in the ion trap mass analyser (with ion trap scan rate of turbo, first mass m/z was 100, AGC Target 5000 and maximum injection time of 35 ms). Data analysis was carried out using Peaks 8.5 (bioinformatics Solutions).

Proximity Ligation Assay

Cells were cultured on 3D-PA gels for 20 hours or 6 days and fixed and processed as described for immunofluorescence before performing Duolink PLA (Sigma Aldrich) as per manufacturer's protocol. Briefly, mouse anti-TWIST1 and rabbit anti-G3BP2 primary antibodies were used to detect endogenous proteins and subsequently recognized using species specific plus and minus PLA oligonucleotide conjugated probes at 37°C for 60 minutes. Interacting probes were then ligated at 37°C for 30 minutes and detected by polymerase mediated amplification at 37°C for 100 minutes and subsequently analysed by fluorescent confocal microscopy. For analysis of formed 5-day acini, a minimum 50 cells from 5 random fields were quantified per condition. To quantify the PLA signal, images were converted to 8-bit images and thresholded, the area of PLA signal was then quantified and normalized to cell number using ImageJ.

Real-time PCR

RNA was extracted from cells using Tri Reagent (Sigma Aldrich). cDNA was generated using random hexamer primers and cDNA Reverse Transcription Kit (Applied Biosystems). Expression values were generated using ddCt values normalized to murine Gapdh or human HPRT. Experiments were performed in biological and technical triplicate. For data analysis in each comparison (one shRNA vs. the control shRNA), unpaired two-tailed Student's T-tests with Welch's correction was used to determine statistical significance.

In Vitro Phosphorylation Assay with Radioactive ATP

Myc-His_6-Twist1 WT and Y107F were pulled down from transfected 293T cells using Ni-NTA agarose resin. Recombinant active LYN was purchased form Sigma. Phosphorylation reactions were carried out in the presence of 100 mM MOPS (pH 7.2), 4 mM free Mg^{2+}, 2.5 mM Mn^{2+} and 50 μg/ml BSA at 37°C. All reactions were carried out in a total volume of 10 μl and quenched with 10 μl of SDS/PAGE loading buffer. Phosphorylated proteins were separated from unreacted ^{32}P-ATP by SDS-PAGE (12% gel), cut from the dried gel and quantified on the ^{32}P channel in liquid scintillant.

In Vitro Cold Phosphorylation Assay

Myc-His_6-Twist1 WT and Y107F were pulled down from transfected 293T cells using Ni-NTA agarose resin. Endogenous LYN or SRC were immunoprecipitated from 3D-cultured MCF10A cells grown on low and high stiffness PA gels for 5 days. Phosphorylation reactions were carried out in the presence of 100 mM MOPS (pH 7.2), 4 mM free Mg^{2+}, 2.5 mM Mn^{2+}, 50 μg/ml BSA and 500 μM ATP at 37°C for 1 hour. Recombinant LYN (Sigma Aldrich) was used as a positive control.

Ni-NTA Purification

Myc-His_6-Twist1 WT and Y107F were pulled down from transfected 293T using HisPur Ni-NTA agarose resin (ThermoFisher). Briefly, cells were lysed using a 2-step lysis protocol as described in the immunoprecipitation section, supplemented with 5mM imidazole. Ni-NTA resin was washed 3 times with lysis buffer containing 5mM imidazole and then incubated with the lysates overnight at 4°C. The resin was then washed 3 times with lysis buffer supplemented with 250mM NaCl and 15mM imidazole, 3 times with lysis buffer supplemented with 250mM NaCl and 30mM imidazole and then eluted in lysis buffer supplemented with 250mM NaCl and 200mM imidazole for 10 minutes at 4°C. The eluates were used for *in vitro* kinase assays or western blots.

Please cite this article in press as: Fattet et al., Matrix Rigidity Controls Epithelial-Mesenchymal Plasticity and Tumor Metastasis via a Mechanoresponsive EPHA2/LYN Complex, Developmental Cell (2020), https://doi.org/10.1016/j.devcel.2020.05.031

Tyrosine Kinases Screen

Wild type (GSPQSYEELQTQRR) and Y107F mutant (GSPQSFEELQTQRR) TWIST1 peptides were synthesized to evaluate the activity of 73 protein kinases. The two peptide substrates were profiled against 73 protein kinases (at 500 μM) using the radiometric assay method (Kinexus, Canada). The intra-assay variability was determined to be less than 10%. A comparison of the difference in counts between the WT and Y107F peptides was analysed as the percentage change from control (Y107F peptide used as control).

Strep-Tactin Pulldown

EPHA2 and LYN cDNAs were transiently transfected into 293AD cells with Lipofectamine 2000 (Life Technologies) according to the recommendations of the manufacturer. Cells were incubated with the DNA-Lipofectamine complexes in Opti-MEM for 4 hours and then the medium was replaced with culture medium. Twenty-four hours after transfection, the cells were washed once with cold PBS containing calcium and magnesium and collected in 300 μl 0.5% TX-100 in PBS with Halt protease and phosphatase inhibitor cocktail (Fisher Scientific), centrifuged at 17,000g at 4C for 10 min, and frozen. For pull-down, cell lysates were precleared at 4°C for 15 min with 20 μl Sepharose 4B beads (Sigma Aldrich) and then incubated at 4°C for 2 hours with 20 μl Strep-Tactin XT Superflow beads (IBA GmbH) on a rotating wheel. The beads were then washed 4 times with cold 0.5% TX-100 in PBS and once with cold PBS. Proteins bound to the beads were eluted in 25 μl Bolt LDS sample buffer (Life Technologies) by heating at 95°C for 2 min. Proteins were separated by SDS-PAGE using Bolt 4-12% Bis-Tris Plus gels (Life Technologies) using Bolt MOPS SDS running buffer (Life Technologies) and transferred to PVDF membranes for immunoblotting using a Bio-Rad Trans-Blot Turbo Transfer System.

Rheology Measurement of Tumor Tissue Stiffness

Samples (normal mouse mammary gland or tumor) were prepared to an individual diameter where each was cut in half and each portion was measured along with major and minor axis with a set of calipers, and thickness of each portion was measured by contact micrometre. An average thickness was used for sample compression. Samples were placed in pairs on opposite sides of porous platens centred at a defined radius, r, of 30 mm. From the average thickness measurement, 20% compression was applied at 0.1 mm/sec, allowed to relax for 10 sec, and then subjected to dynamic shear (±1°, 1 Hz, 10 cycles) with a rotational actuator attached to an Electroforce ELF 3200 system (Bose, Eden Prairie, MN). After testing, samples were snap frozen in liquid nitrogen and stored at -80°C for protein analysis. Biomechanical data were processed to obtain torque amplitude and phase, which were used to determine shear modulus, G. Data were analysed by ANOVA, with significance set at $p < 0.05$. Data are mean ± sd.

Masson Trichrome Staining

5um paraffin-embedded sections were deparaffinized, rehydrated and incubated in Bouin's Solution (Sigma, HT10132) overnight at room temperature. Slides were washed in running tap water, rinsed in distilled water and stain with Weigert's Iron Hematoxylin set (Sigma, HT1079). Slides were washed in running tap water and then the collagen content was stained using the Accustain Trichrome Satin kit (Sigma, HT15). Slides were then dehydrated and mounted in xylene-based Permount. Slides were scanned NanoZoomer Slide Scanner with a 10X objective and tumor area, as well as collagen area, was determined using Image J software.

Xenograft Tumor Assay

1.0×10^6 GFP-labelled MCF10DCIS cells suspended in 15 μl Matrigel (50%, diluted in DMEM/F12) were injected bilaterally into the inguinal mammary fat pads of 6 to 8-week-old female SCID-beige mice CB17.Cg-Prkdc^{scid}Lyst$^{bg\text{-}J}$/Crl. Tumors were allowed to grow for 3 weeks until they reached 5 mm in diameter. Mice were then treated for 21 days with daily oral administration of vehicle control (0.5% Methylcellulose, 0.2% Tween 80) or the dual Bcr-Abl/LYN inhibitor Bafetinib (2.5 or 10mg/kg/day) purchased from Selleckchem. As a negative control group, mice were treated with daily oral administration of vehicle control (4% DMSO, 30% PEG300, 5% Tween 80) or Bcr-Abl specific inhibitor Nilotinib (50 mg/kg/day) purchased from Selleckchem. Mouse weight and tumor sizes were monitored for 6 weeks post tumor cell implantation, until mice were sacrificed and tumor burden analysed. Mice were dissected and tumor invasion assessed *in situ* using a fluorescent dissection scope (Leica Microsystems). All work with animals was performed in accordance with UC San Diego IACUC and AAALAC guidelines.

QUANTIFICATION AND STATISTICAL ANALYSIS

Invasive Acini Quantification

Invasive acini were quantified using brightfield images with at minimum 5 random low-magnification fields being analysed per condition per experiment. Acini were scored as either normally developed acini or acini that adopted a spread and invasive phenotype.

TWIST1 Nuclear Staining Quantification

50-200 individual cells per condition were quantified for TWIST1 nuclear (gated on the DAPI signal) and cytoplasmic mean intensities using ImageJ, and the relative percentage of TWIST1 nuclear staining was calculated. Analysis excluded cells on the edge of the image.

Quantification of IHC Signals from TMAs

Missing and damaged cores, and cores without detectable tumor cells, were omitted from analyses. Cores were scored blindly. Phospho-S897 EPHA2 expression was scored 0 for no detectable expression, 1 for very weak expression, 2 for moderate expres-

Please cite this article in press as: Fattet et al., Matrix Rigidity Controls Epithelial-Mesenchymal Plasticity and Tumor Metastasis via a Mechanoresponsive EPHA2/LYN Complex, Developmental Cell (2020), https://doi.org/10.1016/j.devcel.2020.05.031

sion, 3 for strong expression in 0-75% of tumor cells, and 4 for strong expression in greater than 75% of tumor cells. Phospho-S897 EPHA2 was then divided into pS897^{low} including scores 0, 1 and 2 and pS897^{high} including scores 3 and 4.

Quantification of SHG Signals from TMAs

Images were exported as TIFF files and analysed with CT-FIRE module from the CurveAlign software. The scoring rubric (which was defined prior to blinded scoring) for SHG analysis was defined as ''organized collagen'' in tumors having prominent linearized collagen fibres or as ''disorganized collagen'' in tumors having collagen fibres with high degree of circularity (i.e. curved). we analysed the SHG data using previously described tumor-associated collagen signature (TACS), which correlates with breast tumor aggressiveness (Provenzano et al., 2006): short and curly collagen structures, or TACS-1, are enriched in normal breast tissue or benign tumors; thicker aligned collagen fibres stretch and distribute tangentially to a smooth tumor boundary as tumor grow (TACS-2; 0° angle relative to tumor boundary); in more invasive breast tumors, TACS-3 defines thick collagen fibres, aligned perpendicularly to more irregular tumor boundaries, indicative of areas of local invasion and dissemination (close to 90° angle between collagen fibres and tumor boundary).

Statistical Analysis

Statistical analyses were performed using GraphPad Prism software. All p-values were derived from Student's t-test using unpaired two-tailed analysis with Welch's correction. Error bars denote standard deviation. Kaplan-Meier survival curves were analysed by Cox-Mantel Log-rank analysis using GraphPad Prism software. The correlation between collagen organization or TACS signatures and phopsho-S897 EPHA2 signal in human breast cancer patients' samples (TMA analysis) was analysed using a χ^2 test. Statistical significance was defined as *, ** or *** for $p < 0.05$, $p < 0.01$ or $p < 0.001$, respectively, with regard to the null hypothesis. All qualitative representative data shown were repeated in at least 3 independent biological replicates.

Developmental Cell, Volume *54*

Supplemental Information

Matrix Rigidity Controls Epithelial-Mesenchymal Plasticity and Tumor Metastasis via a Mechanoresponsive EPHA2/LYN Complex

Laurent Fattet, Hae-Yun Jung, Mike W. Matsumoto, Brandon E. Aubol, Aditya Kumar, Joseph A. Adams, Albert C. Chen, Robert L. Sah, Adam J. Engler, Elena B. Pasquale, and Jing Yang

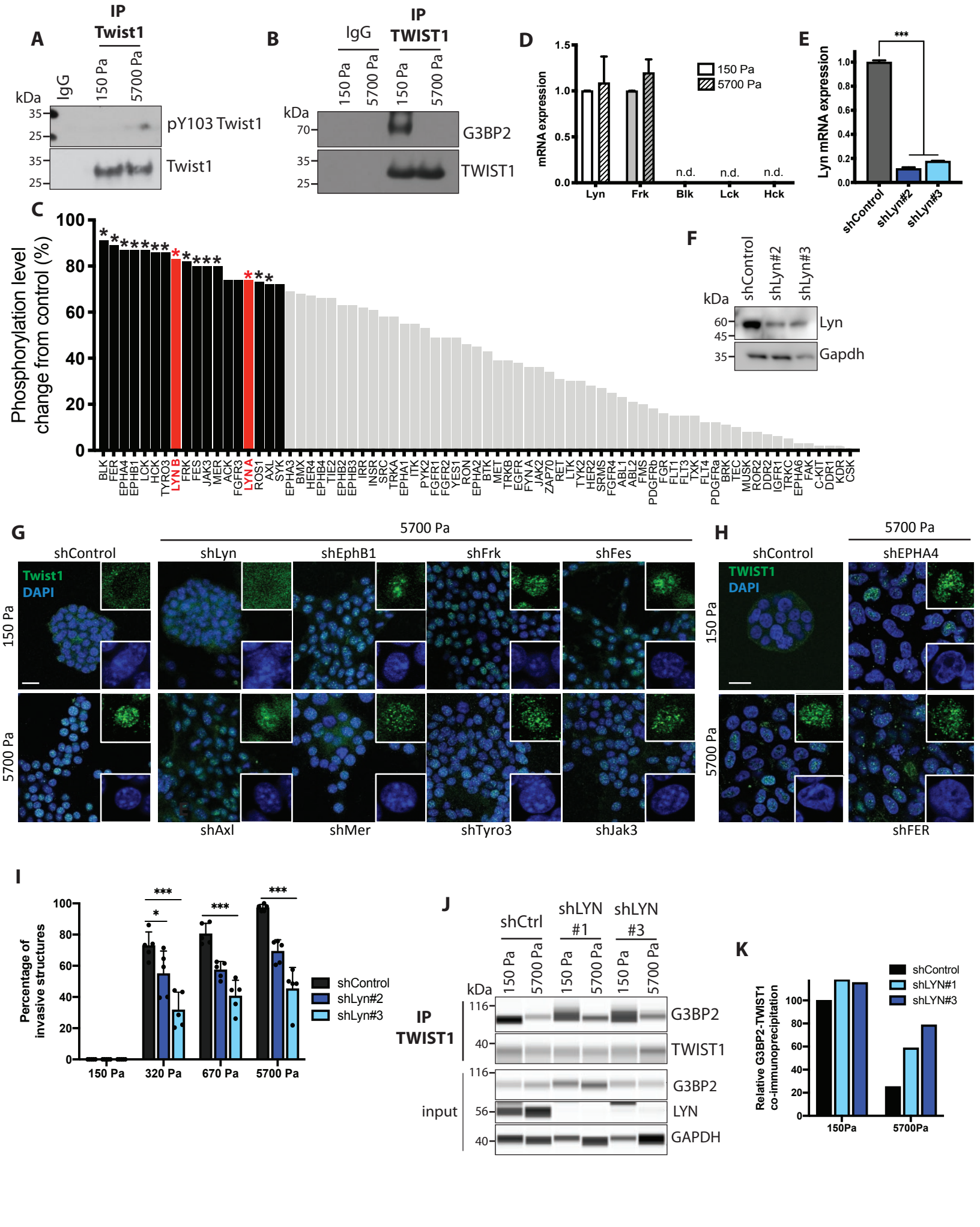
A
IP Twist1
IgG
150 Pa
5700 Pa
kDa
35
25
pY103 Twist1
Twist1
B
IgG
IP TWIST1
150 Pa
5700 Pa
kDa
70
35
25
G3BP2
TWIST1
D
mRNA expression
150 Pa
5700 Pa
Lyn
Frk
Blk
Lck
Hck
n.d.
E
Lyn mRNA expression
***
shControl
shLyn#2
shLyn#3
C
Phosphorylation level change from control (%)
BLK FER EPHA4 EPHB1 LCK HCK TYRO3 LYN B FRK FES JAK3 MER ACK FGFR3 LYN A ROS1 AXL SYK EPHA3 BMX HER4 EPHB4 TIE2 EPHB2 EPHB3 IRR INSR SRC TRKA EPHA1 ITK PYK2 FGFR1 FGFR2 YES1 RON EPHA2 BTK MET TRKB EGFR FYN A JAK2 ZAP70 RET LTK TYK2 HER2 SRMS FGFR4 ABL1 ABL2 FMS PDGFRb FGR FLT1 FLT3 TXK FLT4 PDGFRa BRK TEC MUSK ROR2 DDR2 IGFR1 TRKC EPHA6 FAK C-KIT DDR1 KDR CSK
F
shControl
shLyn#2
shLyn#3
kDa
60
45
35
Lyn
Gapdh
G
5700 Pa
shControl
shLyn
shEphB1
shFrk
shFes
Twist1
DAPI
150 Pa
5700 Pa
shAxl
shMer
shTyro3
shJak3
H
5700 Pa
shControl
shEPHA4
TWIST1
DAPI
150 Pa
5700 Pa
shFER
I
Percentage of invasive structures
***
*
***
***
150 Pa
320 Pa
670 Pa
5700 Pa
shControl
shLyn#2
shLyn#3
J
shCtrl
shLYN #1
shLYN #3
150 Pa
5700 Pa
kDa
IP TWIST1
116
40
G3BP2
TWIST1
input
116
56
40
G3BP2
LYN
GAPDH
K
Relative G3BP2-TWIST1 co-immunoprecipitation
shControl
shLYN#1
shLYN#3
150Pa
5700Pa

Figure S1: LYN regulates TWIST1 nuclear translocation in response to ECM stiffness, Related to Figure 1.

A) Eph4Ras cells were grown on 3D-PA gels with different rigidities for 5 days. Lysates were subjected to Twist1 immunoprecipitation and immunoblotted as indicated.

B) MCF10A cells were grown on 3D-PA gels with different rigidities for 5 days. Lysates were subjected to TWIST1 immunoprecipitation and immunoblotted as indicated.

C) Radiometric Tyrosine kinase screening assay representing the kinase activity as percent change from control. LYN isoforms are highlighted in red. Kinases with CFC > 70% are shown in black. * denotes significance (CFC > 70% and raw values > 10000cpm).

D) Eph4Ras cells were grown on 3D-PA gels with different rigidities for 5 days and RNA was extracted. Bar graph shows mRNA expression relative to control condition (150Pa). n.d.: non-detected.

E) qPCR analysis of relative *LYN* mRNA levels normalized to *HPRT* in EPH4Ras cells as indicated. Data are presented as mean +/- sd, dots represent technical replicates.

F) Immunoblots for LYN and GAPDH in lysate from EPH4Ras cells as indicated.

G) Eph4Ras cells stably expressing control or shRNAs against the top hits from the kinase screening were grown on 3D-PA gels with different rigidities for 5 days, fixed and immunostained for Twist1 (green) and DAPI (blue). Scale bar = 25 μm. Inserts show Twist1 localization at higher magnification.

H) MCF10A cells stably expressing control or shRNAs against EPHA4 or FER were grown on 3D-PA gels with different rigidities for 5 days, fixed and immunostained for TWIST1 (green) and DAPI (blue). Scale bar = 25 μm. Inserts show TWIST1 localization at higher magnification.

I) Eph4Ras cells stably expressing control or Lyn shRNAs were grown on 3D-PA gels with a gradient of increasing rigidities for 5 days. Invasive structures were quantified and represented as percentage. Data are presented as mean +/- sd, dots represent individual fields.

J,K) MCF10A cells were grown on 3D-PA gels with different rigidities for 5 days. Lysates were subjected to TWIST1 immunoprecipitation and immunoblotted as indicated using WES (J), data is quantified in (K).

*** $p < 0.001$; * $p < 0.05$.

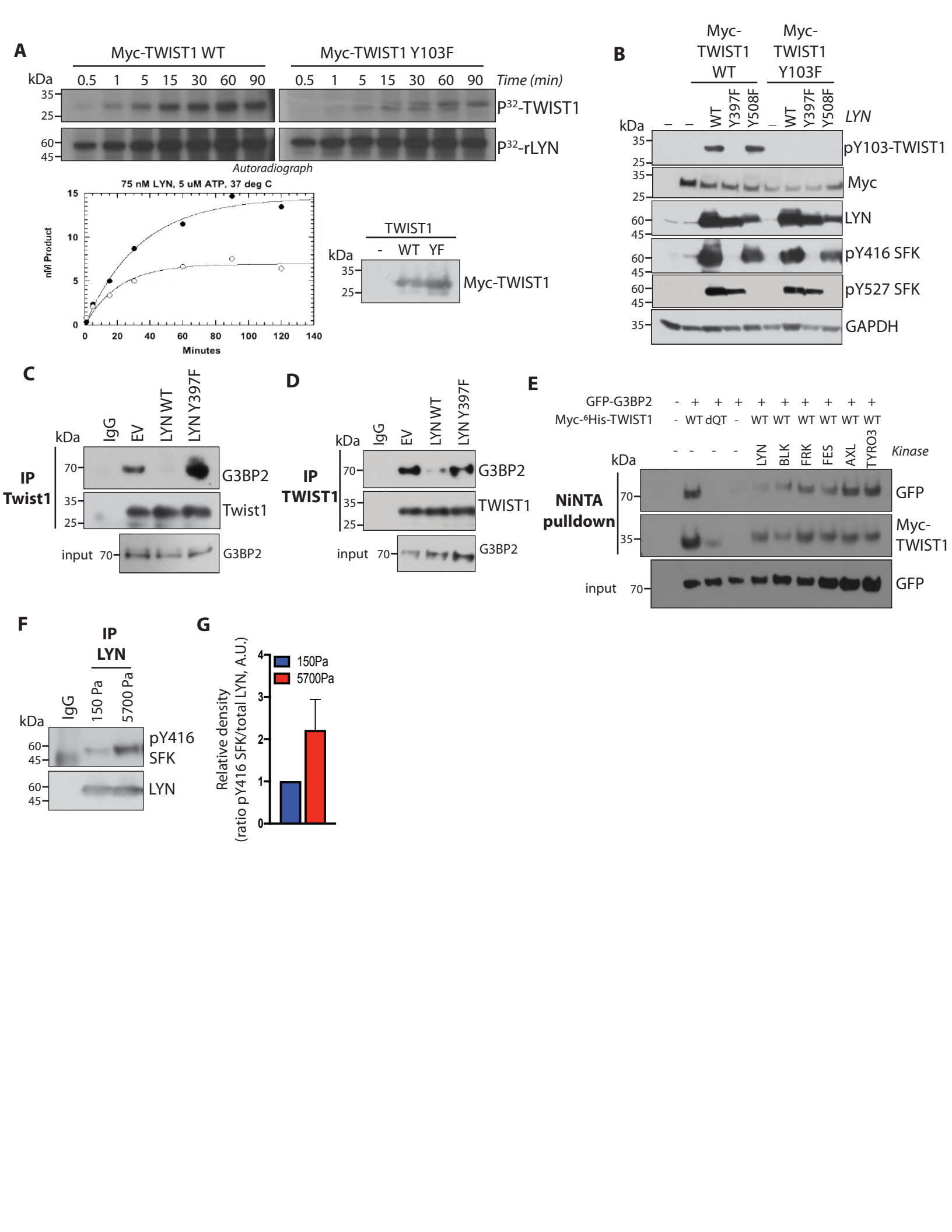
A
Myc-TWIST1 WT
Myc-TWIST1 Y103F
kDa
0.5 1 5 15 30 60 90
0.5 1 5 15 30 60 90
Time (min)
35
25
60
45
P32-TWIST1
P32-rLYN
Autoradiograph
75 nM LYN, 5 uM ATP, 37 deg C
nM Product
Minutes
TWIST1
- WT YF
kDa
Myc-TWIST1
B
Myc-TWIST1 WT
Myc-TWIST1 Y103F
WT Y397F Y508F WT Y397F Y508F
LYN
kDa
pY103-TWIST1
Myc
LYN
pY416 SFK
pY527 SFK
GAPDH
C
IgG EV LYN WT LYN Y397F
kDa
IP Twist1
G3BP2
Twist1
input
G3BP2
D
IgG EV LYN WT LYN Y397F
kDa
IP TWIST1
G3BP2
TWIST1
input
G3BP2
E
GFP-G3BP2
Myc-6His-TWIST1
WT dQT WT WT WT WT WT WT
LYN BLK FRK FES AXL TYRO3
Kinase
kDa
NiNTA pulldown
GFP
Myc-TWIST1
input
GFP
F
IP LYN
IgG 150 Pa 5700 Pa
kDa
pY416 SFK
LYN
G
Relative density (ratio pY416 SFK/total LYN, A.U.)
150Pa
5700Pa

Figure S2: ECM stiffness triggers LYN-dependent TWIST1 phosphorylation on Y103, Related to Figure 2.

A) Upper panel, autoradiograph showing a kinase kinetics assay with recombinant LYN and WT or Y103F mutant Myc-tagged TWIST1 pulled down from 293T cells. Lower left panel, Quantification of P^{32} incorporation, expressed as nM product. Lower right panel, WB control.

B) 293T cells were transfected with Myc-tagged TWIST1 and WT, kinase-deficient (Y397F) and constitutively active (Y508F) mutant LYN constructs. Lysates were immunoblotted as indicated.

C) Eph4Ras cells stably expressing WT or kinase-deficient (Y397F) LYN were subjected to Twist1 immunoprecipitation and immunoblotted as indicated.

D) MCF10DCIS cells stably expressing WT or kinase-deficient (Y397F) LYN were subjected to TWIST1 immunoprecipitation and immunoblotted as indicated.

E) 293T cells were transfected with indicated Myc-His_6-tagged TWIST1 WT or ΔQT (deletion of the G3BP2 binding domain) constructs encoding some of the top hits from the kinase screening and GFP-tagged G3BP2. Lysates were subjected to Ni-NTA purification and immunoblotted as indicated.

F) MCF10DCIS cells were grown on 3D-PA gels with different rigidities for 5 days. Lysates were subjected to LYN immunoprecipitation and immunoblotted as indicated.

G) Relative protein levels in F were quantified by densitometry and presented as a ratio of phospho-Y416 to total LYN levels.

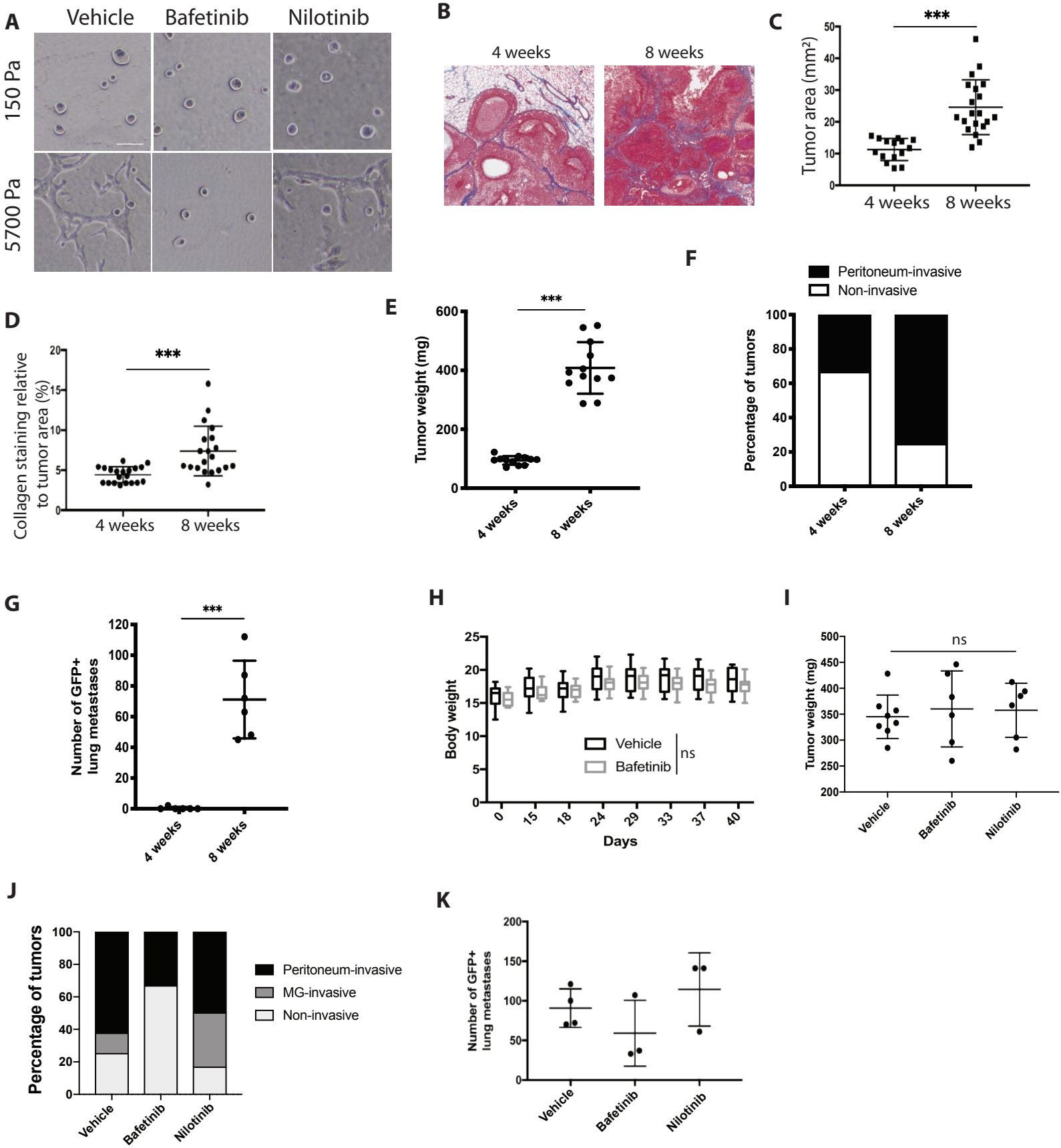
A
Vehicle
Bafetinib
Nilotinib
150 Pa
5700 Pa
B
4 weeks
8 weeks
C
***
Tumor area (mm²)
4 weeks
8 weeks
D
***
Collagen staining relative to tumor area (%)
4 weeks
8 weeks
E
***
Tumor weight (mg)
4 weeks
8 weeks
F
Peritoneum-invasive
Non-invasive
Percentage of tumors
4 weeks
8 weeks
G
***
Number of GFP+ lung metastases
4 weeks
8 weeks
H
Body weight
Vehicle
Bafetinib
ns
Days
I
ns
Tumor weight (mg)
Vehicle
Bafetinib
Nilotinib
J
Percentage of tumors
Peritoneum-invasive
MG-invasive
Non-invasive
Vehicle
Bafetinib
Nilotinib
K
Number of GFP+ lung metastases
Vehicle
Bafetinib
Nilotinib

Figure S3: DCIS to IDC progression correlates with increased invasiveness *in vivo*, Related to Figure 3.

A) MCF10A cells were grown on 3D-PA gels with different rigidities for 5 days in the presence of 1 μM Bafetinib, Nilotinib or vehicle control. Brightfield representative images. Scale bar = 100 μm.

B) Representative images of tumors from MCF10DCIS xenografts harvested at 4 weeks (representing DCIS tumors) or 8 weeks (representing IDC tumors) post injection and analysed for collagen content by trichrome staining.

C) Tumor area (mm^2). Data are presented as mean +/- SD, squares represent individual tumors. N=20 tumors per group.

D) Quantification of collagen content (trichrome staining), expressed as percentage of tumor area. Data are presented as mean +/- SD, dots represent individual tumors. N=20 tumors per group.

E) Tumor weight (mg) is presented as mean +/- SD, dots represent individual tumors. N=12 tumors per group.

F) Regional (peritoneum) invasion of the primary tumor is presented as the percentage of total primary tumors, N=12 tumors per group.

G) Lung metastatic burden is presented as the number of GFP-positive nodules in the lungs. Data are presented as mean +/- SD, dots represent individual animals. N=6 mice per group.

H) Body weight of mice treated with Bafetinib or vehicle control from day 0 to day 40.

I) Tumor weight (mg) at the end of the experiment is presented as mean +/- SD, dots represent individual tumors. Vehicle N=8 tumors, Bafetinib N=6 tumors, Nilotinib N=6 tumors.

J) Local (mammary glands) and regional (peritoneum) invasion of the primary tumor. Data are presented as percentage. Vehicle N=8 tumors, Bafetinib N=6 tumors, Nilotinib N=6 tumors.

K) Lung metastatic burden is presented as the number of GFP-positive nodules in the lungs. Data are presented as mean +/- SD, dots represent individual animals. N=3 (Bafetinib, Nilotinib) or 4 (Vehicle) mice per group.

*** $p < 0.001$; n.s: not significant.

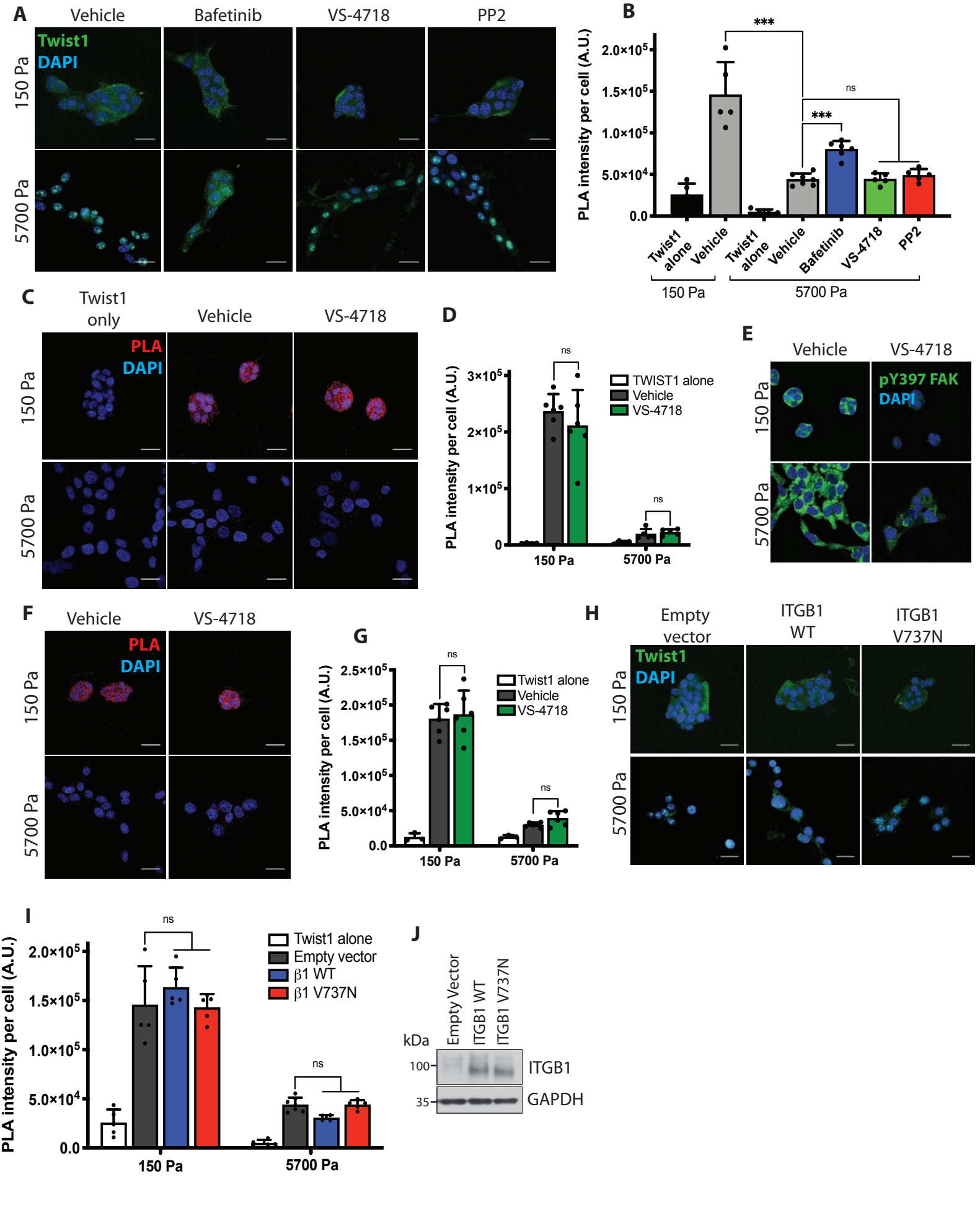
A
Vehicle
Bafetinib
VS-4718
PP2
Twist1
DAPI
150 Pa
5700 Pa
B
PLA intensity per cell (A.U.)
2.0×10^5
1.5×10^5
1.0×10^5
5.0×10^4
0.0
***
ns
***
Twist1 alone
Vehicle
Twist1 alone
Vehicle
Bafetinib
VS-4718
PP2
150 Pa
5700 Pa
C
Twist1 only
Vehicle
VS-4718
PLA
DAPI
150 Pa
5700 Pa
D
PLA intensity per cell (A.U.)
3×10^5
2×10^5
1×10^5
0
ns
ns
TWIST1 alone
Vehicle
VS-4718
150 Pa
5700 Pa
E
Vehicle
VS-4718
pY397 FAK
DAPI
150 Pa
5700 Pa
F
Vehicle
VS-4718
PLA
DAPI
150 Pa
5700 Pa
G
PLA intensity per cell (A.U.)
2.5×10^5
2.0×10^5
1.5×10^5
1.0×10^5
5.0×10^4
0.0
ns
ns
Twist1 alone
Vehicle
VS-4718
150 Pa
5700 Pa
H
Empty vector
ITGB1 WT
ITGB1 V737N
Twist1
DAPI
150 Pa
5700 Pa
I
PLA intensity per cell (A.U.)
2.0×10^5
1.5×10^5
1.0×10^5
5.0×10^4
0.0
ns
ns
Twist1 alone
Empty vector
β1 WT
β1 V737N
150 Pa
5700 Pa
J
kDa
Empty Vector
ITGB1 WT
ITGB1 V737N
100
35
ITGB1
GAPDH

Figure S4: Integrin β1, FAK or SRC signalling are not required for TWIST1 nuclear translocation in response to ECM stiffness, Related to Figure 4.

A) Eph4Ras cells were grown on 3D-PA gels with different rigidities for 3 days in the presence of 1 μM Bafetinib, 500 nM FAK inhibitor VS-4718, 1 μM SRC inhibitor PP2 or vehicle control, fixed and stained for Twist1 (green) and DAPI (blue). Scale bar = 25 μm.

B) Eph4Ras cells were grown as in A), fixed and proximity ligation assay was performed to detect endogenous Twist1-G3bp2 interaction. Quantification of the PLA intensity per cell. A.U.: arbitrary units. Data are presented as mean +/- SD, dots represent individual fields.

C) MCF10A cells were grown on 3D-PA gels with different rigidities for 3 days in the presence of 500 nM FAK inhibitor VS-4718 or vehicle control, fixed and PLA (red dots) was performed to detect endogenous TWIST1-G3BP2 interaction, DAPI is in blue. Scale bar = 25 μm.

D) Quantification of the PLA intensity per cell. A.U.: arbitrary units. Data are presented as mean +/- SD, dots represent individual fields.

E) MCF10A cells were grown on 3D-PA gels with different rigidities for 3 days in the presence of 500 nM FAK inhibitor VS-4718 or vehicle control, fixed and stained for phospho-Y397 FAK (green) and DAPI (blue). Scale bar = 25 μm.

F) Eph4Ras cells were grown on 3D-PA gels with different rigidities for 3 days in the presence of 500nM FAK inhibitor VS-4718 or vehicle control, fixed and PLA (red dots) was performed to detect endogenous Twist1-G3bp2 interaction, DAPI is in blue. Scale bar = 25 μm.

G) Quantification of the PLA intensity per cell. A.U.: arbitrary units. Data are presented as mean +/- SD, dots represent individual fields.

H) Eph4Ras cells stably expressing WT or clustering mutant (V737N) of integrin β1 were grown on 3D-PA gels with different rigidities for 3 days, fixed and stained for Twist1 (green) and DAPI (blue). Scale bar = 25 μm.

I) Eph4Ras cells stably expressing WT or clustering mutant (V737N) of integrin β1 were grown on 3D-PA gels with different rigidities for 3 days, fixed and PLA was performed to detect endogenous Twist1-G3bp2 interaction. Quantification of the PLA intensity per cell. A.U.: arbitrary units. Data are presented as mean +/- SD, dots represent individual fields.

J) Western blot validation of Eph4Ras cells stably expressing WT or clustering mutant (V737N) of integrin β1.

*** $p < 0.001$; ns: not significant.

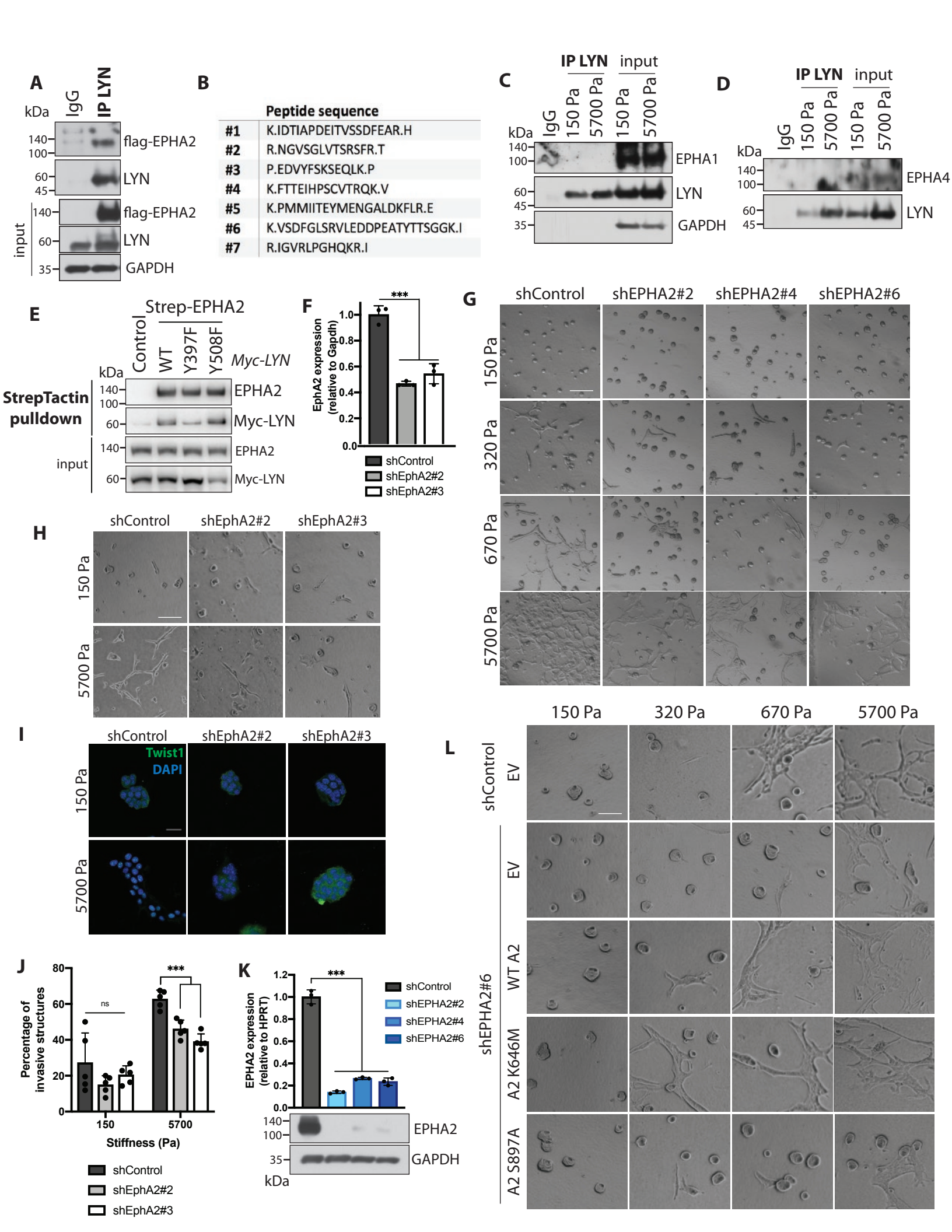
A
kDa
IgG
IP LYN
140
100
flag-EPHA2
60
45
LYN
input
140
flag-EPHA2
60
LYN
35
GAPDH
B
Peptide sequence
#1 K.IDTIAPDEITVSSDFEAR.H
#2 R.NGVSGLVTSRSFR.T
#3 P.EDVYFSKSEQLK.P
#4 K.FTTEIHPSCVTRQK.V
#5 K.PMMIITEYMENGALDKFLR.E
#6 K.VSDFGLSRVLEDDPEATYTTSGGK.I
#7 R.IGVRLPGHQKR.I
C
IP LYN
input
IgG
150 Pa
5700 Pa
150 Pa
5700 Pa
kDa
140
100
EPHA1
60
45
LYN
35
GAPDH
D
IP LYN
input
IgG
150 Pa
5700 Pa
150 Pa
5700 Pa
kDa
140
100
EPHA4
60
45
LYN
E
Strep-EPHA2
Control
WT
Y397F
Y508F
Myc-LYN
kDa
StrepTactin pulldown
140
100
EPHA2
60
Myc-LYN
input
140
EPHA2
60
Myc-LYN
F
***
EphA2 expression (relative to Gapdh)
1.0
0.8
0.6
0.4
0.2
0.0
shControl
shEphA2#2
shEphA2#3
G
shControl
shEPHA2#2
shEPHA2#4
shEPHA2#6
150 Pa
320 Pa
670 Pa
5700 Pa
H
shControl
shEphA2#2
shEphA2#3
150 Pa
5700 Pa
I
shControl
shEphA2#2
shEphA2#3
Twist1
DAPI
150 Pa
5700 Pa
J
Percentage of invasive structures
80
60
40
20
0
ns
***
150
5700
Stiffness (Pa)
shControl
shEphA2#2
shEphA2#3
K
***
EPHA2 expression (relative to HPRT)
1.2
1.0
0.8
0.6
0.4
0.2
0.0
shControl
shEPHA2#2
shEPHA2#4
shEPHA2#6
140
100
EPHA2
35
GAPDH
kDa
L
150 Pa
320 Pa
670 Pa
5700 Pa
shControl
EV
shEPHA2#6
EV
WT A2
A2 K646M
A2 S897A

Figure S5: ECM stiffness-driven LYN activation requires the ephrin receptor EPHA2, Related to Figure 4.

A) 239T cells were transfected with flag-tagged EPHA2. Lysates were subjected to LYN immunoprecipitation and immunoblotted as indicated.

B) Sequences for seven unique EPHA2 peptides from the IP-mass spectrometry experiment found in the high stiffness condition.

C,D) MCF10A cells were grown on 3D-PA gels with different rigidities for 5 days. Lysates were subjected to LYN immunoprecipitation and immunoblotted as indicated.

E) 293AD cells were transfected with indicated constructs and subjected to Strep-Tactin pulldown of Strep-tagged EPHA2 and immunoblotted as indicated.

F) qPCR analysis of relative *EPHA2* mRNA levels normalized to *HPRT* in Eph4Ras cells stably expressing control or EphA2 shRNAs. mRNA expression relative to Gapdh. Data are presented as mean +/- SD, dots represent technical replicates.

G) Representative images of MCF10A cells stably expressing control or EPHA2 shRNAs grown on 3D-PA gels with a gradient of increasing rigidities for 5 days. Scale bar = 200 μm.

H-J) Eph4Ras cells stably expressing control or EphA2 shRNAs were grown on 3D-PA gels with different rigidities for 5 days. H) Representative images. Scale bar = 100 μm. I) Cells were fixed and immunostained for Twist1 (green) and DAPI (blue). Scale bar = 25 μm. J) Quantification of the experiment presented in G as percentage of invasive structures. Data are presented as mean +/- SD, dots represent individual fields.

K) Upper panel, qPCR analysis of relative *EPHA2* mRNA levels normalized to *HPRT* in MCF10DCIS cells as indicated. Data are presented as mean +/- sd, dots represent technical replicates. Lower panel, immunoblots for EPHA2 and GAPDH in lysate from MCF10DCIS cells as indicated.

L) MCF10A cells stably expressing control of EPHA2 shRNA and rescued for the expression of WT, K646M or S897A mutant were grown on 3D-PA gels with a gradient of increased rigidities for 5 days. Representative images. Scale bar = 100 μm.

*** $p < 0.001$; ns: not significant.

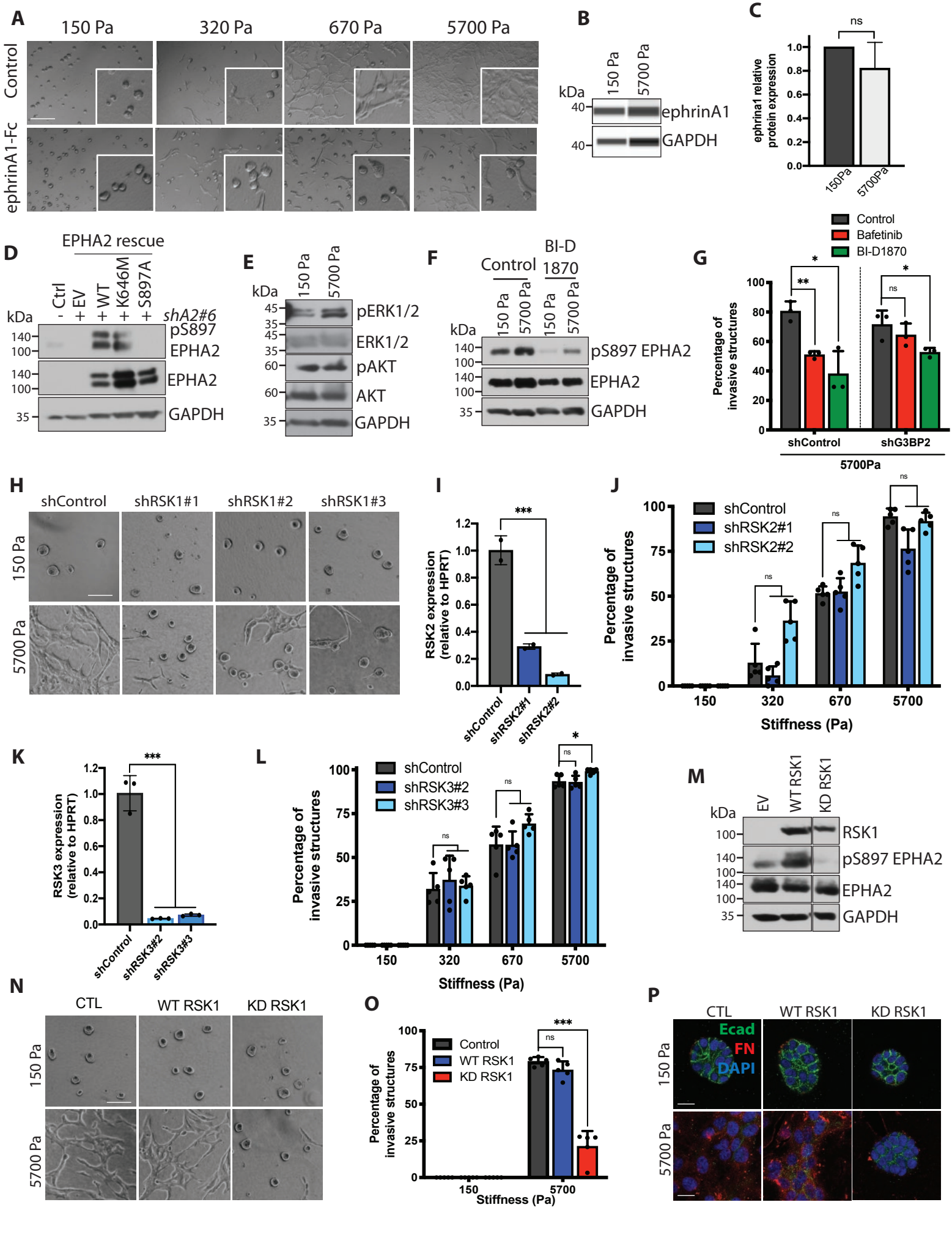
A
150 Pa
320 Pa
670 Pa
5700 Pa
Control
ephrinA1-Fc
B
kDa
150 Pa
5700 Pa
40
ephrinA1
40
GAPDH
C
ns
ephrina1 relative protein expression
1.0
0.8
0.6
0.4
0.2
0.0
150Pa
5700Pa
D
EPHA2 rescue
Ctrl
- EV
+ WT
+ K646M
+ S897A
shA2#6
kDa
140
100
pS897 EPHA2
140
100
EPHA2
35
GAPDH
E
kDa
150 Pa
5700 Pa
45
35
pERK1/2
45
35
ERK1/2
60
pAKT
60
AKT
35
GAPDH
F
Control
BI-D 1870
150 Pa
5700 Pa
150 Pa
5700 Pa
kDa
140
100
pS897 EPHA2
140
100
EPHA2
35
GAPDH
G
Control
Bafetinib
BI-D1870
Percentage of invasive structures
100
80
60
40
20
0
*
**
ns
*
shControl
shG3BP2
5700Pa
H
shControl
shRSK1#1
shRSK1#2
shRSK1#3
150 Pa
5700 Pa
I
***
RSK2 expression (relative to HPRT)
1.2
1.0
0.8
0.6
0.4
0.2
0.0
shControl
shRSK2#1
shRSK2#2
J
shControl
shRSK2#1
shRSK2#2
Percentage of invasive structures
100
75
50
25
0
ns
ns
ns
150
320
670
5700
Stiffness (Pa)
K
***
RSK3 expression (relative to HPRT)
1.2
1.0
0.8
0.6
0.4
0.2
0.0
shControl
shRSK3#2
shRSK3#3
L
shControl
shRSK3#2
shRSK3#3
Percentage of invasive structures
100
75
50
25
0
ns
ns
*
ns
150
320
670
5700
Stiffness (Pa)
M
EV
WT RSK1
KD RSK1
kDa
100
RSK1
140
100
pS897 EPHA2
140
100
EPHA2
35
GAPDH
N
CTL
WT RSK1
KD RSK1
150 Pa
5700 Pa
O
Control
WT RSK1
KD RSK1
Percentage of invasive structures
100
75
50
25
0
***
ns
150
5700
Stiffness (Pa)
P
CTL
WT RSK1
KD RSK1
150 Pa
5700 Pa
Ecad
FN
DAPI

Figure S6: Ligand-independent EPHA2 signalling promotes LYN activation and invasion in response to ECM stiffness, Related to Figure 5 and 6.

A) Representative images from MCF10A cells grown on 3D-PA gels with a gradient of increasing rigidities for 5 days in presence of 400 μg/ml recombinant ephrinA1-Fc chimera or IgG control. Scale bar = 200 μm.

B,C) MCF10A cells were grown on 3D-PA gels with different rigidities for 5 days. B) Lysates were immunoblotted as indicated using WES (B), data is quantified in (C).

D) Immunoblots for EPHA2 and GAPDH in lysate from MCF10A cells stably expressing control or EPHA2 shRNA and rescued for the expression of WT, kinase dead K646M mutant or S897A phosphorylation defective mutant.

E) MCF10A cells were grown on 3D-PA gels with different rigidities for 5 days. Lysates were immunoblotted as indicated.

F) MCF10A cells were grown on 3D-PA gels with different rigidities for 5 days and treated with 5 μM RSK inhibitor BI-D1870 (BID), 1 μM Bafetinib or vehicle control (DMSO). Lysates were immunoblotted as indicated.

G) MCF10A cells stably expressing control or G3BP2 shRNAs were grown on 3D-PA gels with different rigidities for 5 days and treated with 5 μM RSK inhibitor BI-D1870 (BID), 1 μM Bafetinib or vehicle control (DMSO). Cell phenotypes at 5700Pa were quantified as percentage of invasive structures. Data are presented as mean +/- SD, dots represent individual fields.

H) MCF10A cells stably expressing control or RSK1 shRNAs were grown on 3D-PA gels with different rigidities for 5 days. Representative images. Scale bar = 100 μm.

I) qPCR analysis of relative *RSK2* mRNA levels normalized to *HPRT* in MCF10A cells stably expressing control or RSK2 shRNAs. mRNA expression relative to HPRT. Data are presented as mean +/- SD, dots represent technical replicates.

J) MCF10A cells stably expressing control or RSK2 shRNAs were grown on 3D-PA gels with a gradient of increasing rigidities for 5 days. Cell phenotypes were quantified as percentage of invasive structures. Data are presented as mean +/- SD, dots represent individual fields.

K) qPCR analysis of relative *RSK3* mRNA levels normalized to *HPRT* in MCF10A cells stably expressing control or RSK3 shRNAs. Data are presented as mean +/- SD, dots represent technical replicates.

L) MCF10A cells stably expressing control or RSK3 shRNAs were grown on 3D-PA gels with a gradient of increasing rigidities for 5 days. Cell phenotypes were quantified as percentage of invasive structures. Data are presented as mean +/- SD, dots represent individual fields.

M) immunoblots for RSK1 and GAPDH in lysate from of MCF10A cells stably expressing control, WT or RSK1 (K94/447R).

N-P) MCF10A cells stably expressing control, WT or RSK1 (K94/447R) were grown on 3D-PA gels with different rigidities for 5 days. N) Representative images. Scale bar = 100um. O) Cell phenotypes were quantified as percentage of invasive structures. Data are presented as mean +/- sd, dots represent individual fields. P) Cells were fixed and immunostained for E-cadherin
(green), DAPI (blue) and fibronectin (FN, red).

*** $p < 0.001$; * $p < 0.05$; ns: not significant.

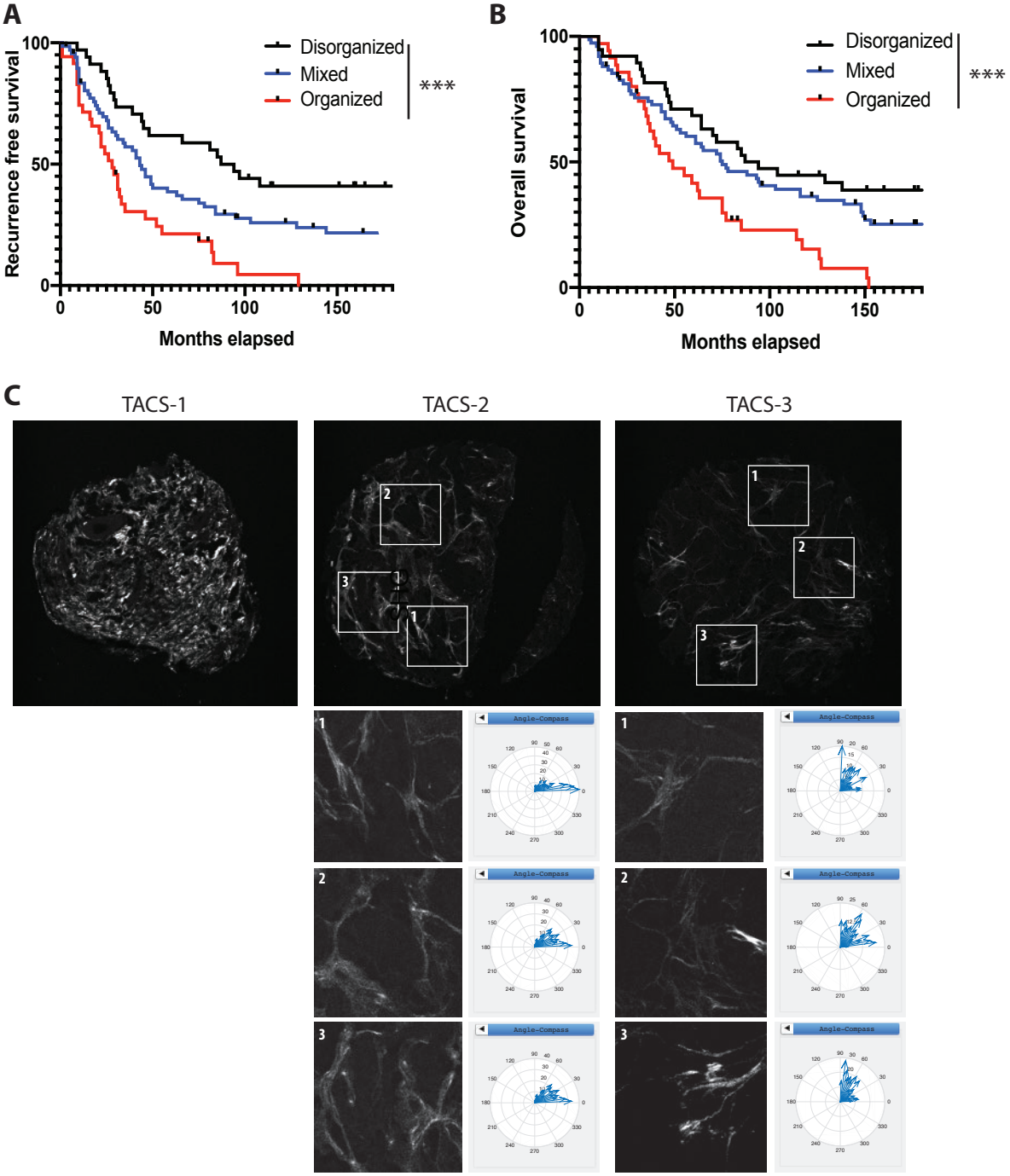
A
Recurrence free survival
100
50
0
0
50
100
150
Months elapsed
Disorganized
Mixed
Organized
***
B
Overall survival
100
50
0
0
50
100
150
Months elapsed
Disorganized
Mixed
Organized
***
C
TACS-1
TACS-2
TACS-3
1
2
3
Angle-Compass

Figure S7: Collagen organization correlates with tumor progression and metastases, Related to Figure 7.

A) Kaplan–Meier curve of recurrence-free survival for stage-3 breast cancer patients, stratified by collagen organization (SHG). N=148 breast tumors (Disorganized N=38; Mixed N=75; Organized N=35).

B) Kaplan–Meier curve of overall survival for stage-3 breast cancer patients, stratified by collagen organization (SHG). N=137 breast tumors (Disorganized N=34; Mixed N=68; Organized N=35).

C) Upper panel, Representative images of stage-3 human breast tumors analysed for TACS scoring by second harmonic generation imaging. Scale bar = 50 μm. Lower panels, left, regions on interest used for analysis of the angle between collagen fibres and tumor boundary. Lower panels, right, compass graphs showing the angle between collagen fibres and tumor boundary. *** $p < 0.001$.

Target	Forward	Reverse
Mouse		
Lyn	ACCCTTATGATGGCATCCAC	GTTGACCTTGGCCACGTAGT
Frk	CAGGGCTACATTCCTTCCAA	CACCCTTCTGGCTCTCACTC
Blk	TGACTCTGCCCTGTGTGAAC	GGTCTTGATGGCCACCTTCA
Lck	GTCCCACTGGACAGCAAGAT	ACCCTTCTCAAAGCCCAAGT
Hck	GCCTCAAAAACAGAGCCAAG	ACAGTGCGACCACAATGGTA
EphA2	GCACAGGGAAAGGAAGTTGTT	CATGTAGATAGGCATGTCGTCC
Gapdh	GACCCCTTCATTGACCTCAAC	CTTCTCCATGGTGGTGAAGA
Human		
EPHA2	AGAGGCTGAGCGTATCTTCAT	GGTCCGACTCGGCATAGTAGA
LYN	GCTTTTGGCACCAGGAAATAGC	TCATGTCGCTGATACAGGGAA
HPRT	GCTATAAATTCTTTGCTGACCTGCTG	AATTACTTTTATGTCCCCTGTTGACTGG
RSK1	TGCACAGCCTGGGTATCATTT	CTGTCCCGCAGAAAGAATAGG
RSK2	GCCACCCTAAAAGTTCGGGAC	TTTCCTTCCGTCTGAAAGGCA
RSK3	CGCTGAGAATGGACAGCAAAT	TCCAAATGATCCCTGCCCTAAT

Table S1: Primers used for qRT-PCR, Related to STAR Methods.

Target	TRC number	Sequence
shControl		CACCGGCAACAAGATGAAGAGCACCAACTCGAGTTGGTGCTCTTCATC TTGTTGTTTTTGAATTC
Mouse		
shLyn#1	TRCN0000023664	CCGGCGCGAGAGTCATCGAAGATAACTCGAGTTATCTTCGATGACTCT CGCGTTTTT
shLyn#2	TRCN0000023666	CCGGGCCAAGGTCAACACCTTAGAACTCGAGTTCTAAGGTGTTGACCT TGGCTTTTT
shLyn#3	TRCN0000023668	CCGGGAGTCACTCATGTGCAAGATTCTCGAGAATCTTGCACATGAGTG ACTCTTTTT
shEphA2#2	TRCN0000023656	CCGGGCCAGTTTAGCCACCACAATACTCGAGTATTGTGGTGGCTAAAC TGGCTTTTT
shEphA2#3	TRCN0000023658	CCGGCGAGGTCATGAAAGCCATCAACTCGAGTTGATGGCTTTCATGAC CTCGTTTTT
shEphB1#1	TRCN0000023499	CCGGGCCTCTTACTAGGAACGGTTTCTCGAGAAACCGTTCCTAGTAAG AGGCTTTTT
shEphB1#2	TRCN0000023500	CCGGCCATCGTGAATGAGACATCTACTCGAGTAGATGTCTCATTCACG ATGGTTTTT
shEphB1#3	TRCN0000023501	CCGGCCAGGCAAGAGGGAAATCTATCTCGAGATAGATTTCCCTCTTGC CTGGTTTTT
shFrk#1	TRCN0000274572	CCGGTACTAATTAGACTGGTTATTCCTCGAGGAATAACCAGTCTAATTA GTATTTTTG
shFrk#2	TRCN0000274515	CCGGTACCACTCCAGTGGCCGTAAACTCGAGTTTACGGCCACTGGAGT GGTATTTTTG
shFrk#3	TRCN0000274574	CCGGTATGACAGGTGCTCAAGTAATCTCGAGATTACTTGAGCACCTGT CATATTTTTG
shFes#1	TRCN0000231270	CCGGCCTAGGCTTCCTGCGACAATACTCGAGTATTGTCGCAGGAAGCC TAGGTTTTTG
shFes#2	TRCN0000231271	CCGGACCCACACTGGAGATCCTTAACTCGAGTTAAGGATCTCCAGTGT GGGTTTTTTG
shFes#3	TRCN0000231272	CCGGGCGTGTACCTCCTCAGCAGTTCTCGAGAACTGCTGAGGAGGTAC ACGCTTTTTG
shAxl#1	TRCN0000322131	CCGGCCAGTCAAGTGGATTGCTATTCTCGAGAATAGCAATCCACTTGA CTGGTTTTTG
shAxl#2	TRCN0000322132	CCGGCGTCAAGGAAATCGGCTGAAACTCGAGTTTCAGCCGATTTCCTT GACGTTTTTG
shAxl#3	TRCN0000322074	CCGGCAGATCCTAGAACTGGCTGATCTCGAGATCAGCCAGTTCTAGGA TCTGTTTTTG
shMer#1	TRCN0000231993	CCGGCTACCTCCTGTTGCGTTTAATCTCGAGATTAAACGCAACAGGAG GTAGTTTTTG
shMer#2	TRCN0000231995	CCGGAGATTTACAGTGGTGATTATTCTCGAGAATAATCACCACTGTAA ATCTTTTTTG
shMer#3	TRCN0000023589	CCGGGCATGAGAGAACCAAGCAAATCTCGAGATTTGCTTGGTTCTCTC ATGCTTTTT
shTyro3#1	TRCN0000023524	CCGGCCTCAGAATTTCCATGCCATTCTCGAGAATGGCATGGAAATTCTG AGGTTTTT
shTyro3#2	TRCN0000023525	CCGGGCCCGATCTTTCAATCGAGAACTCGAGTTCTCGATTGAAAGATC GGGCTTTTT
shTyro3#3	TRCN0000023526	CCGGGCAGCTTGCATGAAGGAGTTTCTCGAGAAACTCCTTCATGCAAG CTGCTTTTT
shJak3#1	TRCN0000279041	CCGGTTCGAGGAGAGACACCTTAAGCTCGAGCTTAAGGTGTCTCTCCT CGAATTTTTG
shJak3#2	TRCN0000297617	CCGGCGGCCTCATTACATCAGATTACTCGAGTAATCTGATGTAATGAG GCCGTTTTTG
shJak3#3	TRCN0000279039	CCGGCCAAGCCACATCTTCTGCATACTCGAGTATGCAGAAGATGTGGC TTGGTTTTTG
Human		

shLYN#1	TRCN0000218210	GTACCGGGGAATCCTCCTATACGAAATTCTCGAGAATTTCGTATAGGAGGATTCCTTTTTTG
shLYN#3	TRCN0000230901	CCGGGAGTGACGATGGAGTAGATTTCTCGAGAAATCTACTCCATCGTCACTCTTTTTG
shEPHA2#2	TRCN0000195734	CCGGGATAAGTTTCTATTCTGTCAGCTCGAGCTGACAGAATAGAAACTTATCTTTTTTG
shEPHA2#4	TRCN0000006403	CCGGCGGACAGACATATAGGATATTCTCGAGAATATCCTATATGTCTGTCCGTTTTT
shEPHA2#6	TRCN0000231648	CCGGTCGGACAGACATATAGGATATCTCGAGATATCCTATATGTCTGTCCGATTTTTG
shFER#1	TRCN0000195272	CCGGCAGAACAACTTAGTAGGATAACTCGAGTTATCCTACTAAGTTGTTCTGTTTTTTG
shFER#2	TRCN0000196348	CCGGGCAGAAAGTTTGCAAGTAATGCTCGAGCATTACTTGCAAACTTTCTGCTTTTTTG
shFER#3	TRCN0000197121	CCGGGCACTGTCCAGAGGATATTTCCTCGAGGAAATATCCTCTGGACAGTGCTTTTTTG
shEPHA4#1	TRCN0000010165	CCGGTCAGTCCGTGTGTTCTATAAACTCGAGTTTATAGAACACACGGACTGATTTTT
shEPHA4#2	TRCN0000220021	CCGGGATTGGCTCCAGGCCATTAAACTCGAGTTTAATGGCCTGGAGCCAATCTTTTTG
shEPHA4#3	TRCN0000332976	CCGGGATTGGCTCCAGGCCATTAAACTCGAGTTTAATGGCCTGGAGCCAATCTTTTTG
shRSK1#1	TRCN0000001384	CCGGAGCGATTCACTGTATAAACTTCTCGAGAAGTTTATACAGTGAATCGCTTTTTT
shRSK1#2	TRCN0000001385	CCGGGCTCTATCTCATTCTGGACTTCTCGAGAAGTCCAGAATGAGATAGAGCTTTTT
shRSK1#3	TRCN0000001388	CCGGGACCATGACACTGATTCTGAACTCGAGTTCAGAATCAGTGTCATGGTCTTTTT
shRSK2#1	TRCN0000006352	CCGGCCAGATTCAAATGAGGAGTAACTCGAGTTACTCCTCATTTGAATCTGGTTTTT
shRSK2#2	TRCN0000011010	CCGGGCCATGAAGGTCCTTAAGAAACTCGAGTTTCTTAAGGACCTTCATGGCTTTTT
shRSK3#2	TRCN0000197173	CCGGGCTCAGCGGAGAGGTATTAAACTCGAGTTTAATACCTCTCCGCTGAGCTTTTTTG
shRSK3#3	TRCN0000194851	CCGGCCGGAATCTATTCGAATTTGTCTCGAGACAAATTCGAATAGATTCCGGTTTTTTG

Table S2: shRNA sequences used in this study, Related to STAR Methods.